Texas A&M University
Mechanical Engineering Department
Turbomachinery Laboratory
Tribology Group

FORCE COEFFICIENTS FOR A LARGE CLEARANCE OPEN ENDS SFD WITH A CENTRAL FEED GROOVE: TEST RESULTS AND PREDICTIONS

Research Progress Report to the TAMU Turbomachinery Research Consortium

TRC-SFD-01-2012

by

Luis San Andrés
Mast-Childs Tribology Professor
Principal Investigator

May 2012

LINEAR-NONLINEAR FORCE COEFFICIENTS FOR SQUEEZE FILM DAMPERS
TRC Project, TEES # 32513/1519 SF

EXECUTIVE SUMMARY

FORCE COEFFICIENTS FOR A LARGE CLEARANCE OPEN ENDS SFD WITH A CENTRAL FEED GROOVE: TEST RESULTS AND PREDICTIONS

LUIS SAN ANDRES, MAY 2012

The report describes a large load Squeeze Film Damper (SFD) test rig[1], details measurements of dynamic loads and circular orbits conducted on a large clearance (c=9.9 mil) open ends centrally grooved SFD, and presents the identified experimental SFD force coefficients for operation at three static eccentricities. The rig has a bearing cartridge supported atop four elastic rods and a stationary journal, rigidly attached to a base structure. The SFD consists of two parallel film lands, one inch in length, separated by a central groove, ½ inch in width and 3/8 inch in depth. In the journal, three equally spaced holes, 120^o apart, supply an ISO VG 2 lubricant into the central groove and squeeze film lands.

The experimental SFD force coefficients are compared to test results obtained earlier with the same land length damper but with a smaller clearance (c=5.55 mil) and against predictions obtained from an advanced physical model that accounts for the flow field in the central groove and the interaction with the adjacent film lands. Dynamic pressures in the film lands and in the central groove are (not) surprisingly of the same order of magnitude. The central groove affects the dynamic forced response of the test damper to generate large direct damping coefficients, ~3.5 times those derived from classical lubrication formulas. Experimental added mass coefficients are ~7.4 times the predictive classical values. Predictions from the advanced model correlate well with the test data when using a shallow effective groove depth.

The measurements and analysis advance understanding of the forced performance of SFDs, point out to the limited value of simplistic predictive formulas, and show the effectiveness of an enhanced predictive tool.

Note: Test data collected by Paola Mahecha, Research Assistant (May 2011). Work funded by Luis San Andrés. Analysis, text and graphical art for 2012 TRC report by Luis San Andrés

[1] Project supported by Pratt & Whitney Engines (2008-2010).

TABLE OF CONTENTS

FORCE COEFFICIENTS FOR A LARGE CLEARANCE OPEN ENDS SFD WITH A CENTRAL FEED GROOVE: TEST RESULTS AND PREDICTIONS

LUIS SAN ANDRES, MAY 2012

LIST OF TABLES

LIST OF FIGURES

Significance of work

High performance turbomachinery demands high shaft speeds, increased rotor flexibility, tighter clearances in the flow passages, advanced materials, and increased tolerance to imbalance [1]. Operation at high speeds induces severe dynamic loading with large amplitude journal motions at the bearing supports. Squeeze Film dampers (SFD) aid to reduce rotor vibrations due to imbalance and other sources and also serve to isolate the rotor(s) from the engine frame or casing [2]. Energy efficient and reliable rotordynamic operation of aircraft engines calls for detailed understanding of the forced performance in actual SFDs. Predictions derived from classical SFD analyses fail to accurately predict the force coefficients for SFDs. It is well known that classical lubrication formulas predict inertia force coefficients that are an order of magnitude lesser than experimental data.

Pratt & Whitney Engines sponsored a two-year experimental and computational program to investigate novel SFD configurations operating at typical conditions encountered in aircraft jet engines. The project provided reliable SFD forced performance data and benchmarked predictions from a new computational program. The program funded the construction of a high load SFD test rig consisting of a rigid journal and an elastically supported bearing cartridge (BC). Two electromagnetic shakers deliver periodic loads to the bearing to induce whirl motions at preset amplitudes and frequencies; max. 500 lb_f and 400 Hz. The test rig permits the excitation of the BC with large amplitude whirl motions of arbitrary shape [3,4]. In practice this is a normal occurrence. However, predicted (linear) SFD force coefficients may not represent with fidelity the actual forced response of a SFD, in particular for off-centered journal motions.

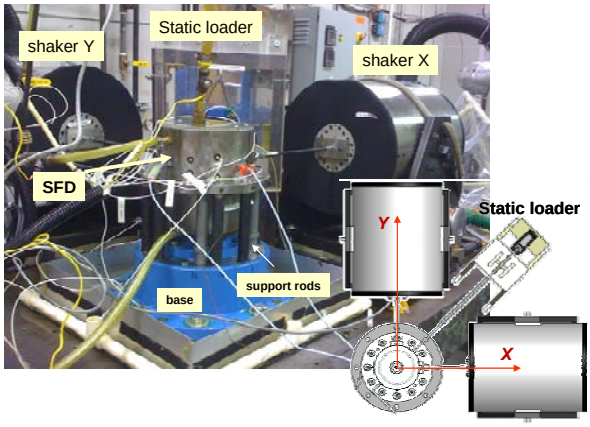

Statement of work and budget

Recall that rotordynamic force coefficients are strictly valid for infinitesimally small amplitude motion about an equilibrium condition. Both requirements, an equilibrium

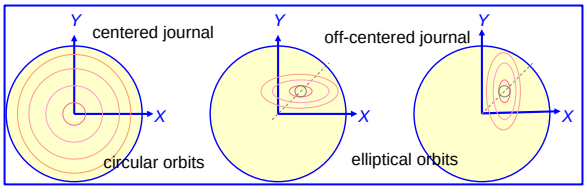

state and small whirl amplitude motions, are often violated in SFD operation.

The proposed work is:

(a) Test the short length open ends damper with dynamic loads (20-300 Hz) inducing off-centered elliptical orbital motions with amplitude ratios as large as 5:1 to reach 80% of the bearing clearance (see inset).
(b) Extract SFD force coefficients from test impedances obtained over a frequency range and correlate coefficients with predictions of linear force coefficients and experimental coefficients for smallest whirl amplitudes (5%*c)*.
(c) Perform computational model numerical experiments, similar to the physical tests, to also extract linearized SFD force coefficients from the nonlinear forces and valid within a frequency range. Determine the goodness of the linear-nonlinear representation from the equivalence in mechanical energy dissipation with the work performed from the actual nonlinear forces (experimental and numerical).

The TRC project was funded in December 2011 with the budget detail listed below. Mr. Sung-Hwa Jung, M.S. graduate student, was hired as a Research Assistant (RA) with an effective start date of January 1, 2012.

BUDGET FROM TRC FOR 2011-2012	**Year I**
Support for graduate student (20 h/week) x $ 1,800 x 12 months	$ 21,600
Fringe benefits (0.6%) and medical insurance ($191/month)	$ 2,419
Travel to (US) technical conference	$ 1,200
Tuition three semesters ($3,802 x 3)	$ 10,138
Supplies for test rig	$ 1,500
Total Cost:	**$ 37,108**

During the last 4 months, the RA has learned about the test rig components and operating procedures, disassembled the test rig and installed, centered and aligned a journal to give a SFD with a nominal 10 mil clearance and lands one inch long, and performed measurements to identify the test system lubricated and dry force coefficients. To the end of May 2012, the expenses amount to $13,687 which include the student salary ($1,950/month) plus social and medical benefits and a modest amount for test rig expenses. For 2012-2013, the amount of $14,000 is requested to continue the project until May 31, 2013.

The report describes the test rig and the measurements obtained by Paola Mahecha, a former graduate student working with the SFD rig. In late April 2012, the current RA repeated the same measurements, obtaining similar results and deriving identical conclusions.

Work will continue throughout 2012 and 2013 to complete the tasks outlined above, in particular with large amplitude orbital motions to determine the validity of the common impedance formulation to derive SFD force coefficients.

Description of large load SFD test rig

Figure 1 shows the PW-SFD test rig and its support structure, a hydraulic static loader and two electromagnetic shakers. Figure 2 depicts the test rig components and their disposition, and Figure 3 presents a schematic view of the SFD test section and the lubricant flow path. The SFD section is the gap between a stationary rigid journal and a bearing cartridge (BC) elastically supported. The journal with diameter D=127 mm is rigidly mounted to a base, which in turn is fastened to a heavy pedestal. Twelve steel rods (4 main rods and 8 flexural rods) support the BC to give an isotropic structural static stiffness (K_S).

A hydraulic static loader positioned 45^o away from the X and Y axes serves to statically displace the BC to an off-centered or eccentric position. Two electromagnetic shakers orthogonally positioned along the X and Y axes connect, through slender stingers, to the BC for delivery of periodic loads at preset frequencies and amplitudes.

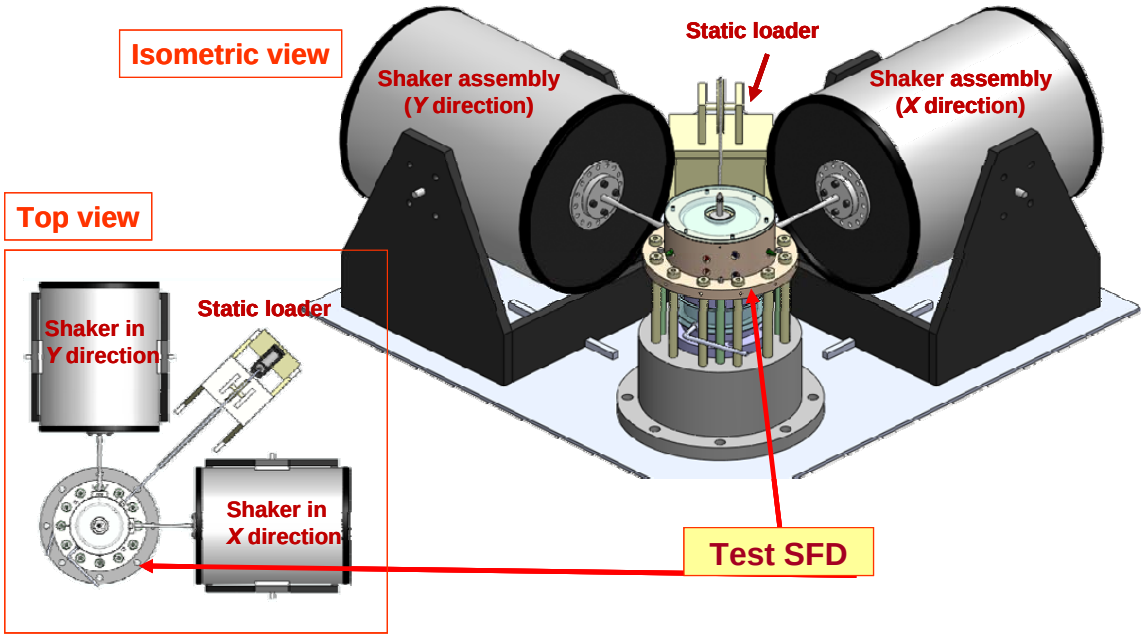

Fig. 1 Top and side views of the PW SFD test rig.

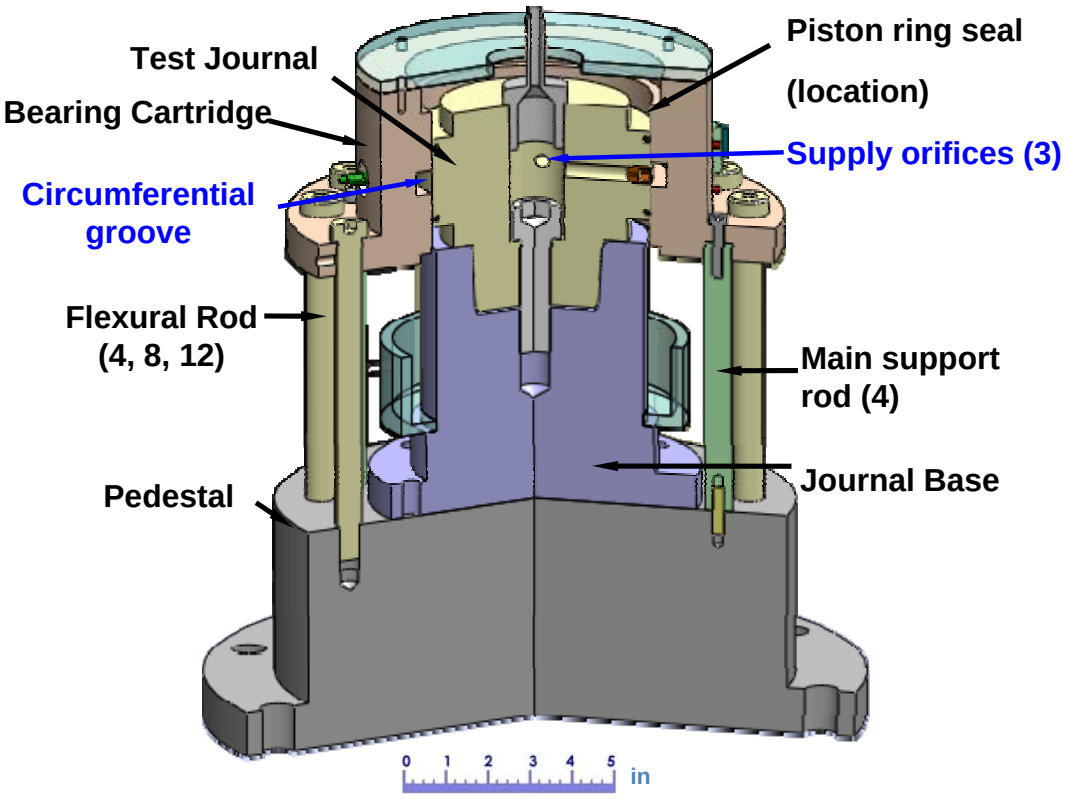

Fig. 2. Cross-section view of test SFD with long journal. [3]

The journal is hollow to route lubricant from a supply system to the SFD through three orifice restrictors, each 2.54 mm in diameter and 120° apart. When installed, the nominal radial clearance between the journal and BC is c~0.025 mm (0.010 in). The BC with inner diameter D+2c contains a groove of width and depth equal to L_G=12.7 mm and d_G=9.5 mm. Hence, as shown in Figure 3, there are two squeeze film lands of length L=25.4 mm (1 in), above and below the central groove.

Table 1 lists the dimensions of the damper and the measured radial clearance c~0.0251 mm (9.9 mil). Note that the groove depth is ~ 38 times the film thickness (clearance) in the damper lands. The lubricant used is ISO VG 2 oil whose viscosity at room temperature is similar to that of an aircraft jet engine lubricant at its operating condition (~ 200° C).

Note also that the number of active (open) orifice holes can be varied by selective plugging. The journal incorporates end grooves for installation of piston seal rings, if needed. Incidentally, the number of elastic rods supporting the BC can be varied from four to 16, and thus the support stiffness can be tailored within a distinctive range, from K_S=4.38 MN/m to

26.3 MN/m (25 klb$_f$/in to 150 klb$_f$/in). Presently, as depicted in Figure 4, twelve rods support the BC.

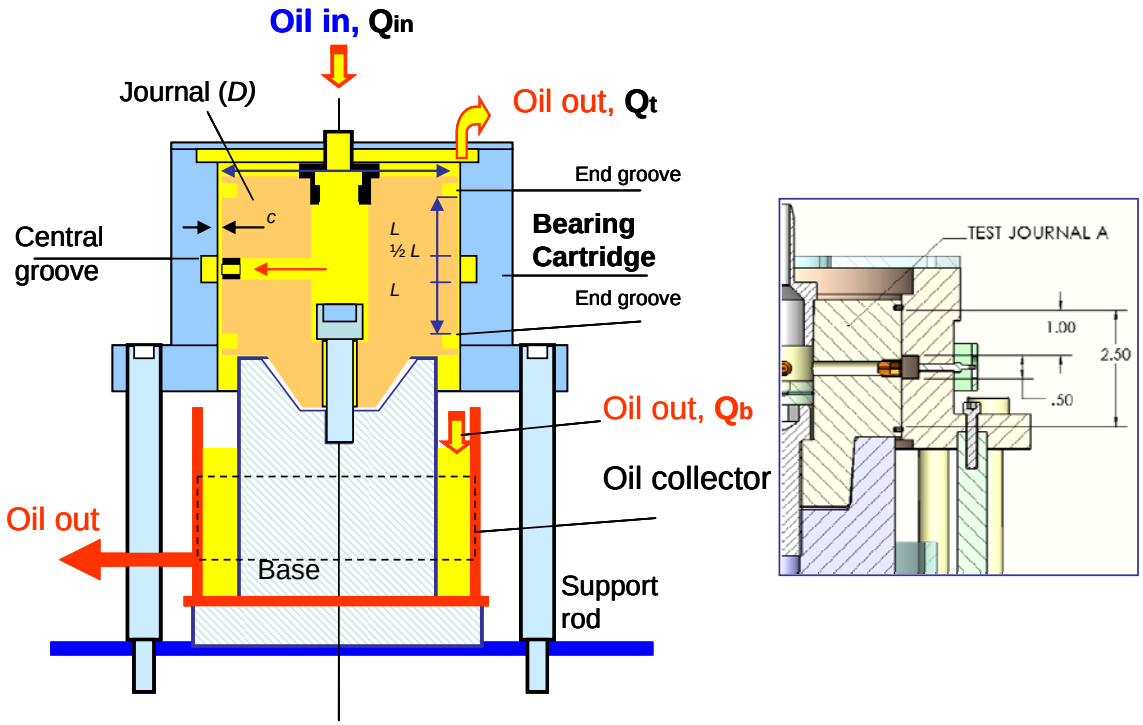

Fig. 3 Cross section view of SFD test rig and lubricant flow path through damper film lands.

Table 1. Geometry and oil properties for test open ends SFD.
Nominal radial clearance c=0.254 mm (10 mil).

	SI unit	US Unit
Journal diameter, D	127 mm	5 inch
Land length, L	25.4 mm	1 inch
Radial clearance, c	0.251 mm	9.9 mil
Groove axial length, L_G	12.7 mm	0.5 inch
depth, d_G	9.5 mm	3/8 inch
Oil wetted length, $2L+L_G$	63.5 mm	2.5 inch
Groove static pressure, P_G	0.11 bar	1.6 psig
Oil inlet temperature, T_S	23 °C	73 °F
Lubricant	**ISO VG 2**	
Density, ρ	785 kg/m^3	49 lb/ft^3
Viscosity μ at T_S	0.0031 Pa.s	0.45 micro-Reynolds
Flow rate, Q_{in}	5.00 LPM	1.32 GPM

Max. static load (1.556 kN: 350 lb$_f$),
Max. amplitude dynamic load (2,000 kN: 440 lb$_f$)
Range of excitation frequencies: 35-250 Hz

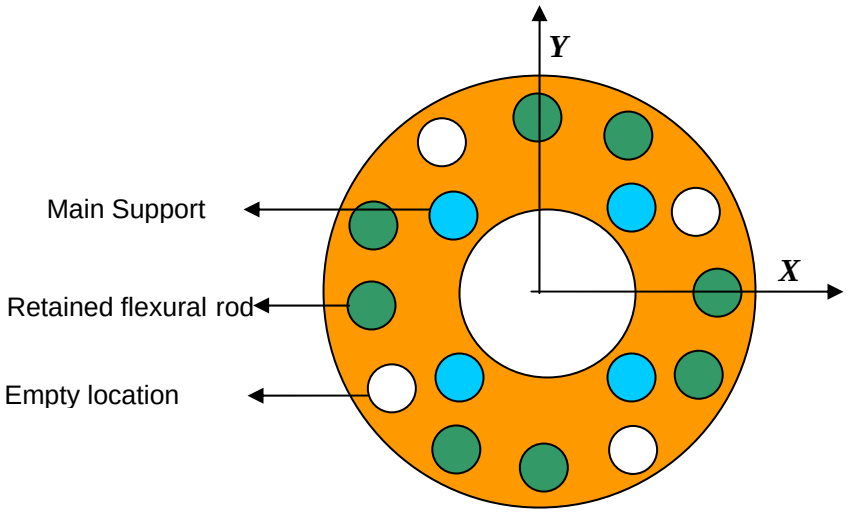

Fig. 4 Disposition of support rods holding bearing cartridge.

The test rig was constructed for a funded research program that aimed to deliver reliable experimental SFD data and to develop an experimentally benchmarked and accurate SFD forced performance predictive tool for integration in an engineering process handling the rotordynamics design and analysis of jet engine performance. Several students, graduate and undergraduate, worked in a fast paced project which delivered as intended in spite of the severe economic crunch of the late 2000's. The test schedule included dynamic load measurements with two film two land lengths (short and long), four support stiffnesses, two film radial clearances, and two end conditions (open and sealed).

The research team prepared 23 technical progress reports and comprehensive annual reports. Near 1,500 dynamic load tests were conducted on short and long journals, with open ends and sealed conditions for increasing static eccentricities, whirl amplitudes and frequencies, lubricant feed pressure and varying the number of active feed holes. The bearing dynamic motions imposed include unidirectional, circular and elliptical orbits. Note also that a comprehensive LABview® DAQ system and a Mathcad® data post-processing code for parameter identification were developed for the project.

Refs. [3, 4] are student M.S. theses relevant to the project. Seshaghiri [3] details the test rig operation, parameter identification procedure, and reports SFD force coefficients for two open ends configurations with two film land lengths, 0.5 inch and 1.0 inch. Mahecha [4] continued the work and tested piston ring end sealed SFDs, extended the parameter

identification procedure, and showcased comparisons of her results with those for the open ends SFD coefficients in Ref. [3]. San Andrés, Principal Investigator, developed the predictive software for SFDs performing arbitrary orbital motions and based on earlier seminal work in the Turbomachinery Laboratory [5,6]. Recently, San Andrés [7] compiled a technical paper summing the test results in Ref. [3].

Identification of structural parameters for dry test system

In general, upon installation and centering of a (new) journal or reconfiguration of the rods' support system the process calls for the measurement of the support structure static stiffness (K_S). To this end, static pull loads are imposed on the dry (unlubricated) structure displacing the BC radially to a maximum eccentricity e_S~0.35c (3.5 mil).

Figure 5 shows the static load versus the BC displacement and the estimated static structure stiffness K_S~17.5 MN/m (100 klb$_f$/in) from a linear curve-fit of the test data. Note that the BC off-center displacement is 45^o away from the X and Y axes.

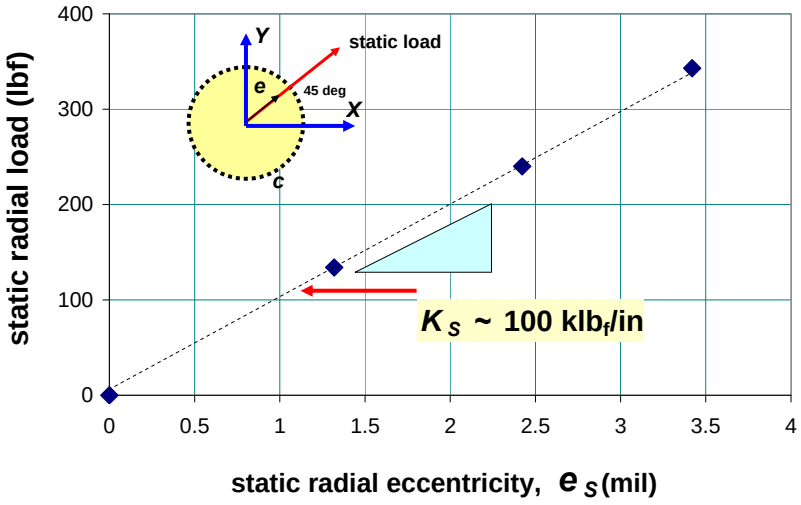

Fig. 5. Static pull load vs. BC radial displacement (e_S). Bearing supported on 12 rods. Structure static stiffness K_S~100 klb$_f$/in

Still under dry (no lubricant) conditions and with a centered BC, single-frequency loads are exerted on the BC to induce circular orbits of amplitude r=15.2 μm (0.6 mil). The

dynamic loads $\mathbf{F}_{(t)}=\{F_X,\ F_Y\}^T$, BC accelerations $\mathbf{a}_{(t)}=\{a_X,\ a_Y\}^T$, and BC displacements $\mathbf{z}_{(t)}=\{x,y\}^T$ relative to the journal are recorded for each frequency (ω) and processed for estimation of the system parameters using an ad-hoc computational software implementing the Instrument Variable Filter Method (IVFM) [8].

In the frequency domain, the equations of motion of the unlubricated or dry test system are

$$\left(\mathbf{K}_s + i\,\omega\mathbf{C}_s - \omega^2\,\mathbf{M}_s\right)\overline{\mathbf{z}}_{(\omega)} = \overline{\mathbf{F}}_{(\omega)} - \mathbf{M}_{\mathbf{BC}}\overline{\mathbf{a}}_{(\omega)} \qquad (1)$$

where $i=\sqrt{-1}$, and for example $\overline{\mathbf{a}}_{(\omega)} = DFT\left[\mathbf{a}_{(t)}\right]$ is the discrete Fourier transform of the acceleration vector. Above **(K, C, M)$_s$** stand for the matrices of structural force coefficients. Note that $-\omega^2\,\overline{\mathbf{z}}_{(\omega)} \neq \overline{\mathbf{a}}_{(\omega)}$ at excitation frequencies > 130 Hz [4]; hence the identification method must treat the BC displacement $\mathbf{z}_{(t)}$ and the acceleration $\mathbf{a}_{(t)}$ as independent variables.

From Eq. (1), impedance coefficients $\mathbf{H}_s$ and flexibility coefficients $\mathbf{G}_s$ for the structure are defined as

$$\mathbf{H}_s = \mathbf{K}_S - \omega^2\mathbf{M}_s + i\,\omega\mathbf{C}_S\,, \quad \mathbf{G}_s = \mathbf{H}_s^{-1} \qquad (2)$$

Table 2 lists the identified test (dry) system structural force coefficients from tests spanning a frequency range of 50-210 Hz. Figure 6 depicts typical system flexibility coefficients $G_{ij} = \dfrac{\partial X_i}{\partial F_j},\ _{i,j=X,Y}$ (amplitude and phase) versus excitation frequency for circular orbit tests conducted with an off-centered journal (e_S=3 mil).

Table 2. Structural parameters of dry test system (bearing cartridge and support assembly) derived from circular centered orbits. Frequency range 50 Hz-210 Hz

Bearing Structure		Direct ***XX***	Direct ***YY***	Cross ***XY***	Cross ***YX***
Stiffness	K_s [klb$_f$/in]	107.3	120.1	-0.5	-0.4
Damping	C_s [lb$_f$-s/in]	8.4	8.8	0.0	-0.3
Mass	M_s [lb]	-3.8	-3.2	-0.3	0.4
System Mass	M_{BC} [lb]	48.0	48.0		
Natural frequency	f_{ns} [Hz]	148	156		
Damping ratio	ξ_s	0.036	0.036		

Static stiffness of structure K_S = 100 klb$_f$/in

The test results for the dry-structure evidence little structural cross-coupling, i.e., $\left(K_{s_{XY}}, K_{s_{YX}}\right) << \left(K_{s_{XX}}, K_{s_{YY}}\right)$ Recall that the static structural stiffness K_S=100 klb$_f$/in while the structural stiffnesses derived from the circular orbit tests $\left(K_{s_{XX}}, K_{s_{YY}}\right)$ are different. $K_{s_{XX}}$ and $K_{s_{YY}}$ are 7% and 20% higher that the static stiffness magnitude. The different stiffnesses also cause a change in the natural frequencies of the dry-system structure.

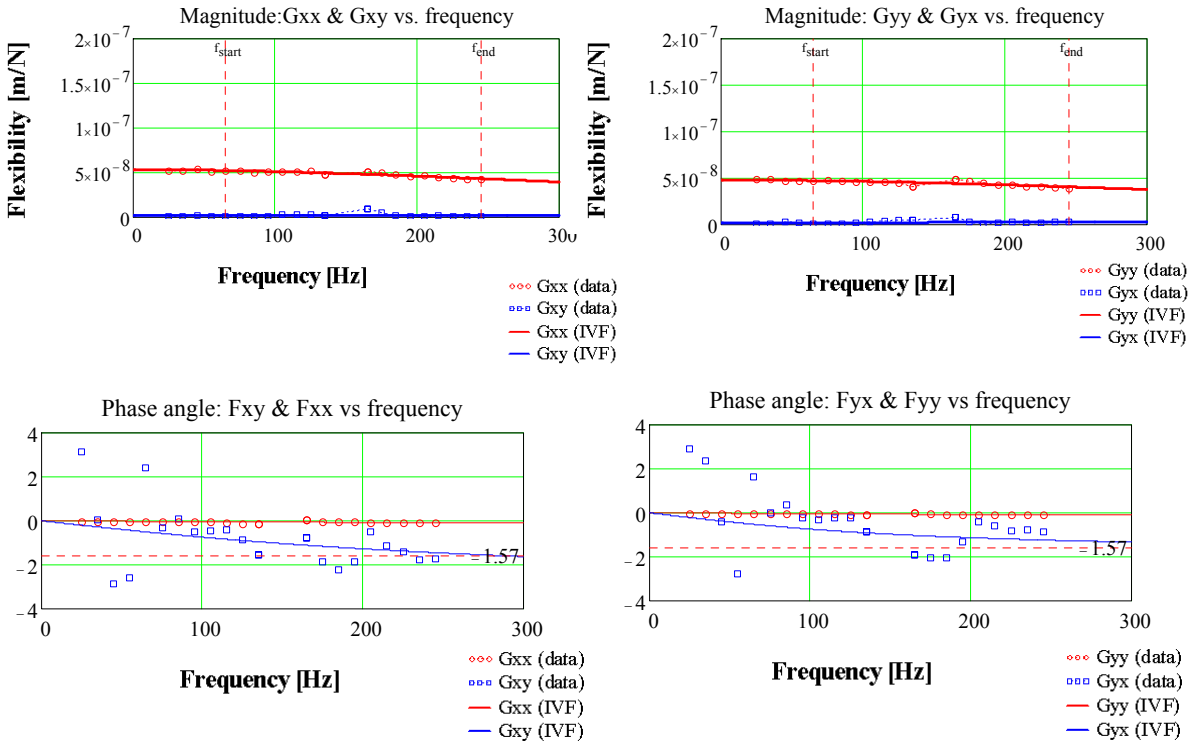

Fig. 6 Amplitude and phase angle of flexibility functions (G_{ij}) vs. excitation frequency for dry (unlubricated) test system. Experimental values and model curve fits. Identification range 50 – 210 Hz. Open ends damper with *c*=9.9 mil and one inch land lengths. Off-centered journal (e_S=3 mil), circular orbits *r* =0.5 mil.

Identification of force coefficients with lubricated test system

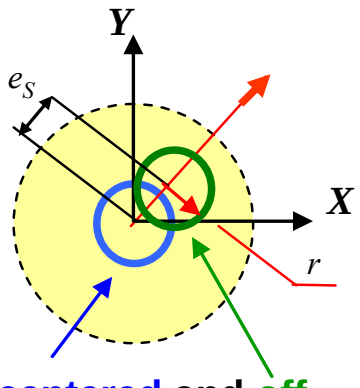

centered and off-centered circular orbits

Lubricant ISO VG 2 is supplied at an inlet pressure of 0.11 bar (1.6 psig) and temperature of ~73 ^{o}F (~23^{o}C). The recorded flow rate at this supply condition is ~1.32 GPM (5.00 LPM). Flow rates for various other oil supply pressures are listed later.

During tests with the BC at its centered position (e_S=0) and at three static eccentricities e_S= 1, 2 and 3 mil (75 μm) displaced with the static loader, the dynamic load shakers induced single frequency (50-250 Hz) circular orbits of the BC with amplitude r=0.5 mil (12.5 μm) , as shown in the inset graph to the left. The BC static displacements (e_S) are 45^{o} away from the X and Y axes.

The equations of motion for the lubricated test system in the frequency domain become

$$\left(\left[\mathbf{K_S}+\mathbf{K_{SFD}}\right]+i\,\omega\left[\mathbf{C_S}+\mathbf{C_{SFD}}\right]-\omega^2\left[\mathbf{M_S}+\mathbf{M_{SFD}}\right]\right)\bar{\mathbf{z}}_{(\omega)}=\bar{\mathbf{F}}_{(\omega)}-\mathbf{M_S}\bar{\mathbf{a}}_{(\omega)} \qquad (3)$$

where $\mathbf{(K, C, M)_{SFD}}$ represent the matrices of squeeze film damper force coefficients (stiffness, damping and inertia).Eq. (3) can also be written as

$$\left(\mathbf{H}_{\mathbf{s}_{(\omega)}}+\mathbf{H}_{\mathbf{SFD}_{(\omega)}}\right)\bar{\mathbf{z}}_{(\omega)}=\mathbf{H}_{\mathbf{LUB}_{(\omega)}}\,\bar{\mathbf{z}}_{(\omega)}=\bar{\mathbf{F}}_{(\omega)}-\mathbf{M_S}\bar{\mathbf{a}}_{(\omega)} \qquad (4)$$

where

$$\mathbf{H_{SFD}}=\mathbf{K_{SFD}}-\omega^2\mathbf{M_{SFD}}+i\,\omega\mathbf{C_{SFD}} \qquad (5)$$

is the matrix of SFD impedance coefficients.

Table 3 lists the identified force coefficients for the lubricated test system, i.e., the parameters add the SFD force coefficients to the dry-structure parameters. Cross-coupled force coefficients are small, relative to the direct force coefficients, for most test conditions except those with the largest static off-center BC displacement (e_S=3 mil).

Appendix A shows characteristic flexibility coefficients $G_{ij}=\dfrac{\partial X_i}{\partial F_j},_{\,i,j=X,Y}$ (amplitude and phase) for the tests with the lubricated system. The appendix also presents the real and imaginary parts of the impedance coefficients for scrutiny of the correlation between the assumed physical model and the test data.

Table 3. Force coefficients of lubricated test system from circular orbits: centered (e_S=0) and three off-center positions (e_S=1, 2 and 3 mil). Open ends SFD with c=9.90 mil and one inch land lengths. Frequency range 50 – 250 Hz

Static eccentricity e_S (mil)	Static load (lbf)	Whirl amplitude, r (mil)	Identified Direct Coefficients					
			K_{XX} (klb$_f$/in)	K_{YY} (klb$_f$/in)	M_{XX} (lb)	M_{YY} (lb)	C_{XX} (lb$_f$-s/in)	C_{YY} (lb$_f$-s/in)
0.0	0	0.5	105.7	118.7	23.6	26.6	38.7	43.5
1.0	108	0.5	106.1	119.1	23.8	26.4	43.2	45.3
2.0	216	0.5	105.2	115.8	25.3	27.0	42.3	46.8
3.0	324	0.5	137.1	231.6	28.2	35.1	56.4	61.1
TABLE 2	**DRY**	**SYSTEM**	107.3	120.8	-3.8	-3.2	8.4	8.8

Static eccentricity e_S (mil)	Static load (lbf)	Whirl amplitude, r (mil)	Identified Cross-Coupled Coefficients					
			K_{XY} (klb$_f$/in)	K_{YX} (klb$_f$/in)	M_{XY} (lb)	M_{YX} (lb)	C_{XY} (lb$_f$-s/in)	C_{YX} (lb$_f$-s/in)
0.0	0	0.5	-1.7	-3.6	1.1	1.4	5.0	4.1
1.0	108	0.5	0.7	-3.9	1.2	0.6	6.8	7.1
2.0	216	0.5	0.0	-1.1	1.5	1.8	4.9	5.8
3.0	324	0.5	60.0	51.7	5.7	5.7	13.1	14.2
TABLE 2	**DRY**	**SYSTEM**	-0.5	-0.4	-0.3	0.4	0.0	-0.3

The experimental SFD force coefficients

Table 4 gives the SFD coefficients derived by subtracting the dry system structural force coefficients from the lubricated system force coefficients, i.e.

$$(\mathbf{K, C, M})_{SFD} = (\mathbf{K, C, M})_{lubricated} - (\mathbf{K, C, M})_{s} \quad (6)$$

Note that the reported SFD force coefficients represent the combined action of the two parallel film lands (top and bottom) and the central groove. In general, the SFD cross-film force coefficients are small relative to the direct force coefficients. Note also that C_{XX}~C_{YY} and M_{XX}~M_{YY}, as expected from the circumferential symmetry of the test SFD system. In addition, the SFD direct stiffnesses are a minute fraction of the test system structural stiffness. However, the test results at e_S=3 mil are suspect, i.e., the data results are anomalous. That is, the assumed physical model (*K, C, M*) shows little correlation with the experimental data. Refer to Appendix B for the uncertainty of the experimental force coefficients as well as the

goodness of the curve fits for the assumed physical model reproducing the experimental data within a specific excitation frequency range.

Table 4. Open ends SFD force coefficients derived from circular orbits: centered (e_S=0) and three off-center positions (e_S=1, 2 and 3 mil). Frequency range 50 – 250 Hz. Damper with *c*=9.90 mil clearance and one inch land lengths.

Static eccentricity e_S (mil)	Static load (lbf)	whirl amplitude, r (mil)	SFD Direct Coefficients					
			K_{XX} (klb$_f$/in)	K_{YY} (klb$_f$/in)	M_{XX} (lb)	M_{YY} (lb)	C_{XX} (lb$_f$-s/in)	M_{YY} (lb$_f$-s/in)
0.0	0	0.50	-1.6	-1.4	27.4	29.8	30.3	34.7
1.0	108	0.50	-1.2	-0.9	20.0	23.3	34.9	36.9
2.0	216	0.50	-2.1	-4.3	21.4	23.9	34.0	38.4
3.0	324	0.50	29.8	111.6	24.4	31.9	48.1	52.8

Static eccentricity e_S (mil)	Static load (lbf)	whirl amplitude, r (mil)	SFD Cross-Coupled Coefficients					
			K_{XY} (klbf/in)	K_{YX} (klbf/in)	M_{XY} (lb)	M_{YX} (lb)	C_{XY} (lbf-s/in)	C_{YX} (lbf-s/in)
0.0	0	0.50	-1.2	-3.2	1.5	0.9	5.1	4.4
1.0	108	0.50	1.1	-3.5	1.6	0.2	6.8	7.4
2.0	216	0.50	0.4	-0.7	1.8	1.4	4.9	6.2
3.0	324	0.50	60.4	52.2	6.0	5.3	13.1	14.5

Comparison of force coefficients for two open ends SFDs, small and large clearances (*c*~5.5 and 9.9 mil)

Seshaghiri [3] reports the SFD force coefficients for two open ended dampers with film land lengths equaling L= 0.5 inch and 1.0 inch and with a nominal clearance of 5 mil (actual c=5.55 mil). Presently, the test results from Seshaghiri are compared against the present ones obtained with a larger film clearance, c=9.90 mil, and identical film land lengths (L=25.4 mm =1 inch).

For reference, Table 5 lists the distinct operation characteristics for the tests conducted with the two dampers, both with same film length and differing film land clearances.

Table 5. Operating conditions for tests with open ends SFDs (one inch land lengths) and two film clearances

Actual clearance c (mil)	Structure static stiffness K_S (klb$_f$/in)	Whirl amplitude r (mil)	Static Groove pressure P_G (psig)	Inlet flow rate Q_{in} (GPM)	Frequency range (Hz)
5.55	150 (*)	0.5	10.2	1.80	50-250
9.90	100	0.5	1.70	1.36	110-250

(*) The test SFD configuration in Ref. [3] had 16 rods in place to support the BC.

Figure 7 shows the SFD direct damping and inertia force coefficients versus static eccentricity (e_S) for two dampers with the same film length but differing clearances. Note that the force coefficients are derived from circular orbit tests.

As expected, the damping and inertia force coefficients are larger for the damper with the tightest clearance. The damping coefficients $(C_{XX},\ C_{YY})_{SFD}$ for the damper with small clearance(c=5.5 mil) are ~3.7 times that for the large clearance (c=9.9 mil) damper. The added mass coefficients $(M_{XX},\ M_{YY})_{SFD}$ appear to double when the clearance increases from c=5.5 to 9.9 mil.

For an open ends SFD with a centered journal, the classical damping (C*) and inertia (M*) coefficients are [2]

$$C^* = C^*_{XX} = C^*_{YY} = 2\times 12\,\pi\,\mu\,L\left(\frac{D}{2c}\right)^3\left[1-\frac{\tanh\left[L/D\right]}{L/D}\right]$$

$$M^* = M^*_{XX} = M^*_{YY} = 2\times \pi\,\rho\,\frac{L}{c}\left(\frac{D}{2}\right)^3\left[1-\frac{\tanh\left[L/D\right]}{L/D}\right] \qquad (6)$$

The formulas above are valid for a full film condition, i.e., without lubricant cavitation, and for infinitesimally small amplitude journal motions. The predicted SFD force coefficients using the formulas in Eq. (6) give

c=5.5 mil $\quad C_*$= 7,121 kNs/m (40.6 lb$_f$.s/in) $\quad M_*$= 2.98 kg (6.58 lb$_m$)

c=9.9 mil $\quad C_*$= 1,255 kNs/m (7.16 lb$_f$.s/in) $\quad M_*$= 1.67 kg (3.69 lb$_m$)

The theoretical force coefficients are a fraction of the identified coefficients, in particular the added mass coefficients. The generation of fluid dynamic pressures in the central groove is paramount to augment substantially the test SFD damping and inertia force coefficients.

From classical lubrication theory [2] for short length bearings damping coefficients are proportional to $(L/c)^3$ while added mass coefficients are proportional to (L/c). Since the dampers' film land lengths (L=1 inch) are identical, then the expected ratios for the force coefficients are

$$\frac{M_{c=5.55\text{mil}}}{M_{c=9.90\text{mil}}}=\left(\frac{9.90}{5.55}\right)=1.78 \;\; ; \;\; \frac{C_{c=5.55\text{mil}}}{C_{c=9.90\text{mil}}}=\left(\frac{9.90}{5.55}\right)^3=5.67 \tag{7}$$

From test results at the centered condition (e_S=0); see Figure 7, the ratios of the added masses and damping coefficients for the two dampers are

$$\begin{aligned} &\left(\frac{M_{c=5.55\text{mil}}}{M_{c=9.90\text{mil}}}\right)_{XX}=2.04; \;\; \left(\frac{M_{c=5.50\text{mil}}}{M_{c=9.90\text{mil}}}\right)_{YY}=1.70 \\ &\left(\frac{C_{c=5.55\text{mil}}}{C_{c=9.90\text{mil}}}\right)_{XX}=3.86; \;\; \left(\frac{C_{c=5.55\text{mil}}}{C_{c=9.90\text{mil}}}\right)_{YY}=3.57 \end{aligned} \tag{8}$$

The test results show the added masses scale well with $(1/c)$; however, the damping force coefficients are not proportional to $1/c^3$. The rationale for the difference lies on the effect of the central groove (and feed holes) on affecting the dynamic force coefficients. In other words, the theory addresses to a simple damper model while the test damper has two distinctive characteristics: three feed holes, 120^o apart, and a deep central groove.

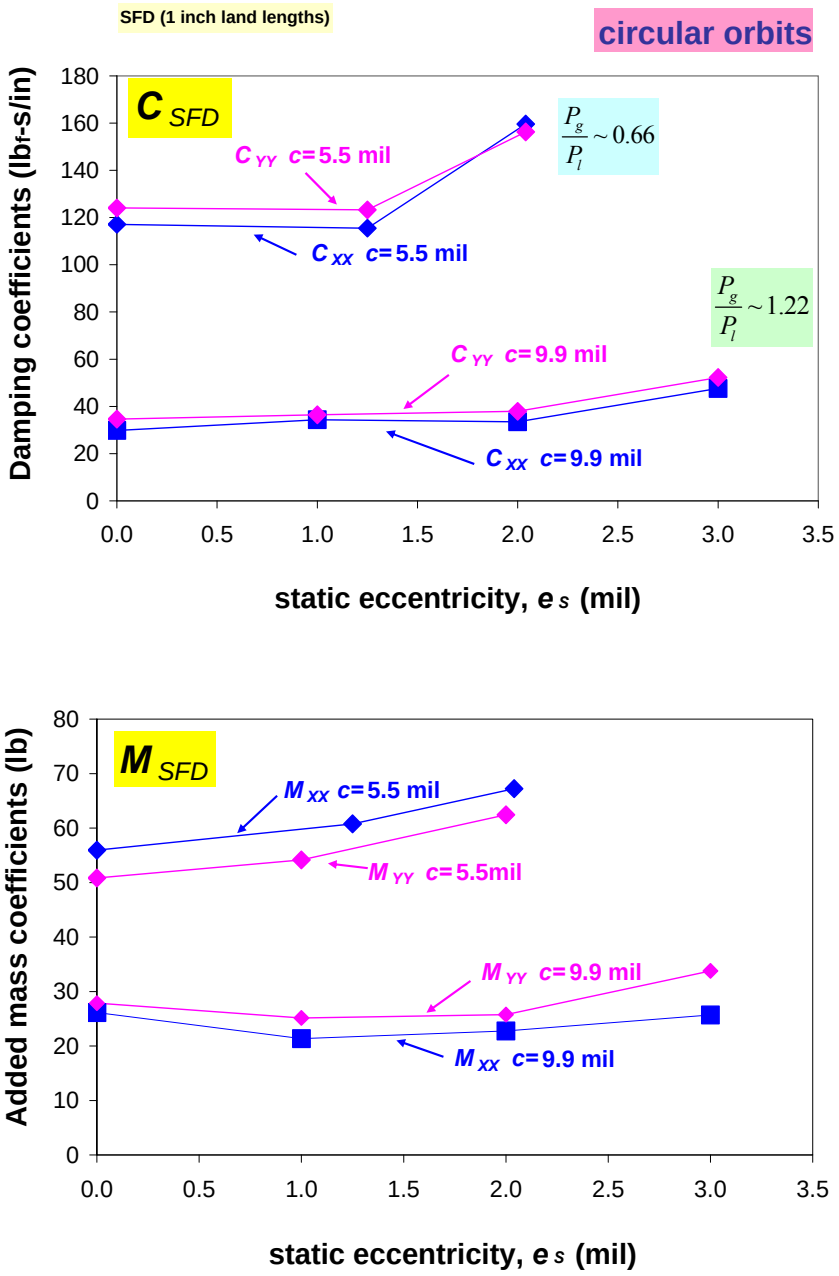

Fig. 7 Open ends SFDs: Direct damping (C_{XX}, C_{YY})$_{SFD}$ and inertia (M_{XX}, M_{YY})$_{SFD}$ coefficients versus static eccentricity (e_S). Film radial clearances c~5.5 mil [3] and 9.9 mil. Orbit radius amplitude r=0.5 mil. One inch film land lengths.

The significant discrepancy between theoretical and experimental results is not unusual. Please refer to prior relevant work by San Andrés [2] and Delgado and San Andrés [5] and San Andrés and Delgado [6], and more recently the theses of Seshaghiri [3] and Mahecha [4].

Dynamic film pressures recorded in the film lands and groove of test damper

Figure 8 depicts the six piezoelectric pressure sensors installed in the bearing cartridge to measure lubricant pressures at mid-axial length of the squeeze film lands and in the central deep groove. In the top and bottom lands there are two pairs of sensors installed 120° apart. Two other sensors measure dynamic pressures in the central groove. The sensor disposition changes with the journal land lengths, one inch for the long damper and ½ inch for the short one [3,4]. The sensors are flush mounted to the inner diameter of the bearing cartridge and thus face directly into the film land or central groove.

This section presents the amplitude of peak-peak dynamic pressures recorded in the damper central groove and in the film lands. During the dynamic load tests, the lubricant film pressures are periodic with a fundamental frequency equaling that of the excitation frequency. See Refs. [3,4] for more test data showing the time variation of the film and groove pressures.

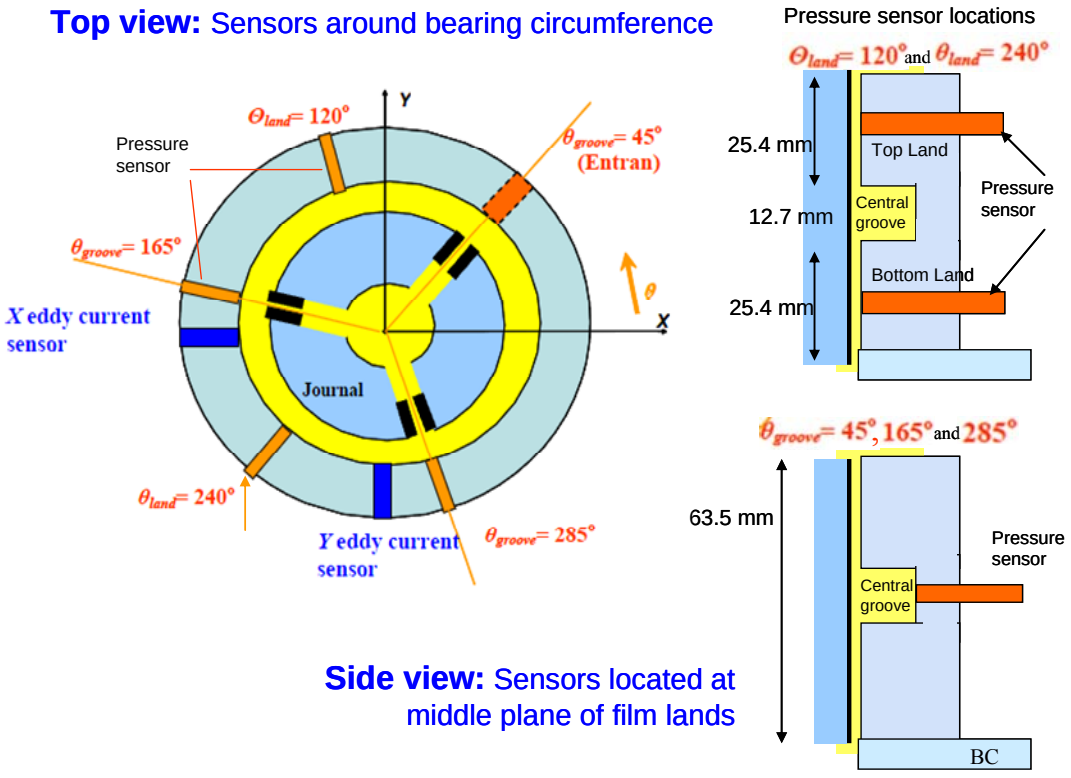

Fig. 8 Disposition of dynamic pressure sensors in bearing cartridge. Damper with one inch lands lengths.

For the open ends SFDs with film clearances c=9.9 mil and c=5.5 mil, Figure 9 illustrates the effect of excitation frequency on the peak to peak (p-p) dynamic pressures recorded in the film lands (P_l), top and bottom, and in the central groove (P_g) at two circumferential locations. The p-p film pressures for the damper with the small clearance are more than twice larger than those for the damper with the large clearance. Note that the groove dynamic pressures are not negligible.

The measurements demonstrate that the deep central groove does not isolate adjacent film lands and is not a region of constant pressure! In actuality, the measurements make evident that the dynamic pressures in the central groove are as substantive as those in the film lands. In actuality, for the damper with the larger clearance (c=9.9 mil), the dynamic pressures in the groove are even higher than those in the film lands. The effect is evident in Figure 10 that shows the ratio of groove to film land peak to peak pressures (P_g/P_l) versus excitation frequency.

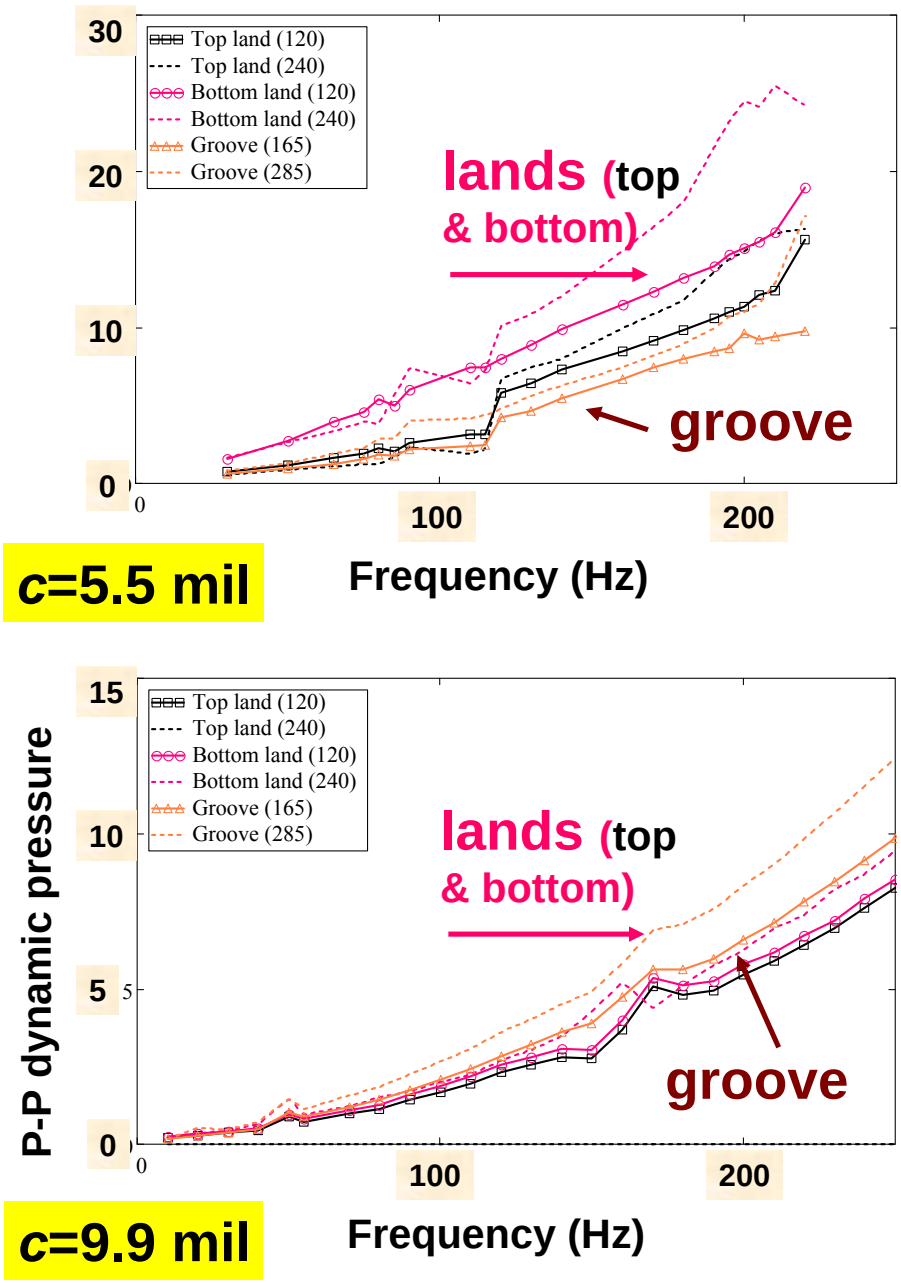

Fig. 9 Peak to peak dynamic pressures at film lands (θ = 120° and 240°, top and bottom) and central groove (θ =165°, 285°) vs. excitation frequency. Centered bearing, e_S=0. Open ends SFD with one inch land lengths and two film clearances (a) c = 5.55 mil (b) c= 9.90 mil.

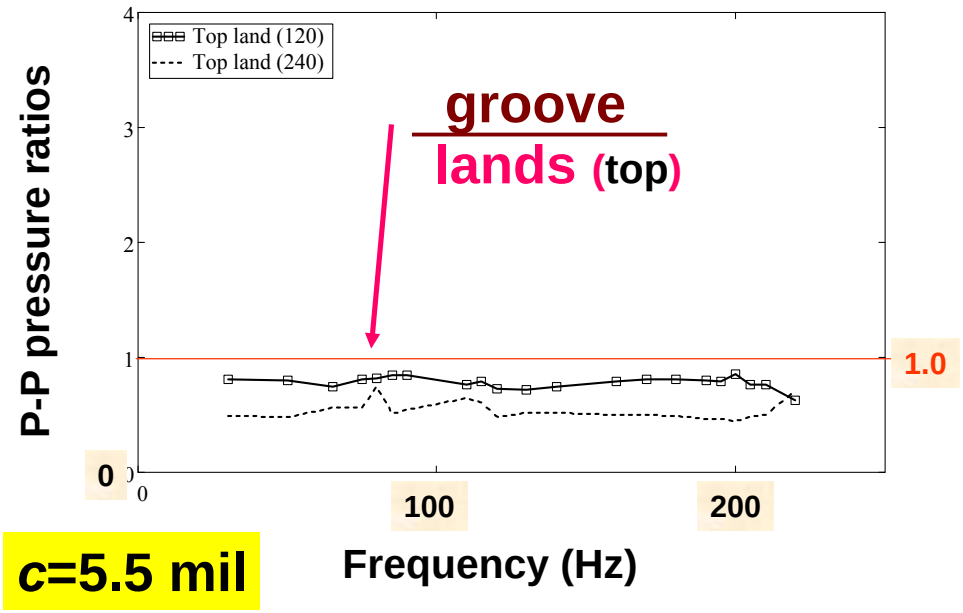

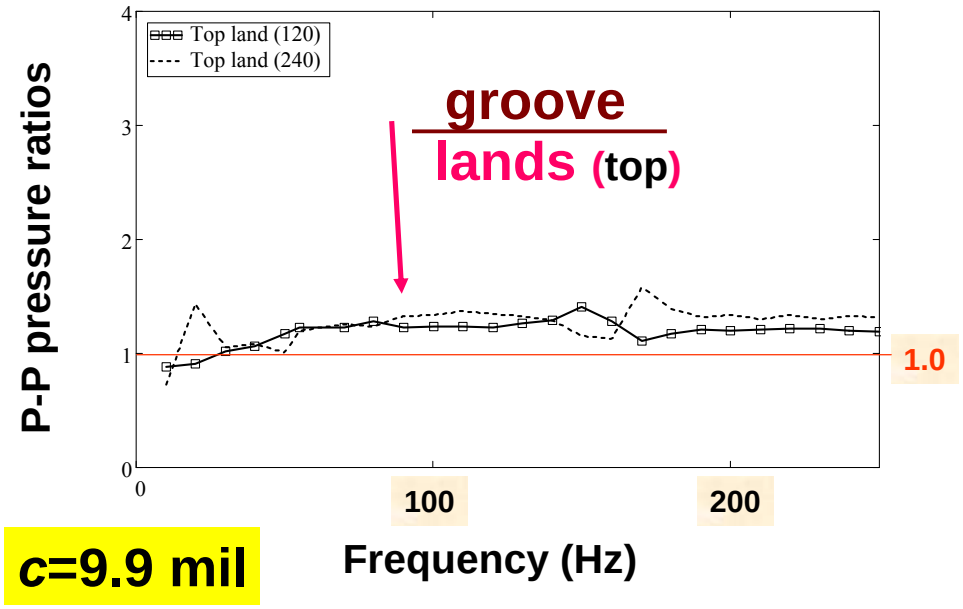

Fig. 10 Ratio of groove to land peak-peak dynamic pressures vs. excitation frequency. Centered bearing, e_S=0. Open ends SFD with one inch land lengths and two film clearances (a) *c* = 5.55 mil (b) *c* = 9.90 mil.

Measurements of flow rate and flow conductances

For the two open ends SFDs, clearances c=5.55 mil and c= 9.90 mil, Table 6 lists the measured lubricant flow rates at the damper inlet (Q_{in}) and through the bottom land flow (Q_b) for increasing magnitudes of the static pressure recorded in the central groove (P_G). Note that for a perfectly centered and aligned damper BC and with a uniform clearance Q_b/Q_{in}=0.50. The table also lists the flow conductances, i.e., the ratio of flow rate to pressure drop across a film land, $C_c=Q/P_G$.

Table 6. Measured lubricant flow rates (inlet and through bottom land) and static pressure in central groove for two open ends dampers with film clearances (a) c=9.9 mil (b) c=5.5 mil [3]. One inch film land lengths.

a) c=9.90 mil					b) c=5.5 mil			
P_G psig	Q_{in} GPM	Q_b GPM	Ratio b/in		P_G psig	Q_{in} GPM	Q_b GPM	Ratio b/in
1.50	1.18	0.64	0.54		6.5	1.2	0.6	0.50
1.70	1.36	0.77	0.56		8.1	1.5	0.7	0.47
2.1	1.76	0.98	0.56		10.2	1.8	0.8	0.44
GPM/psi	**0.814±0.02**	**0.453**	**0.56**	**Flow Conductance**	GPM/psi	**0.181±0.02**	**0.084**	**0.47**

As expected, the damper with a larger clearance "leaks" more than the SFD with a tighter clearance. This damper has a lesser flow resistance or higher flow conductance, C~0.45 GPM/psi, while the damper with small clearance has C~0.08 GPM/psi for the bottom film lands. The ratio of flow conductances (large/small clearances) is ~5.4.

On the other hand, for a simple or idealized damper with film length (L) and with uniform feed pressure on one end and ambient pressure on the other end, the axial flow conductance (C) is [2]

$$\frac{Q}{\Delta P}=C=\frac{\pi D c^3}{12\mu}\frac{1}{L} \qquad (9)$$

From the Eq. above, theory delivers a ratio of flow conductances $\frac{C_{c=9.90\text{mil}}}{C_{c=5.55\text{mil}}}=\left(\frac{9.90}{5.55}\right)^3=5.65$, similar in magnitude to that of the measurements.

However, using the simple formula in Eq. (9) delivers poor predictions for the measured flow rates; that is $C_{c=9.9\text{mil}}$=0.735 GPM/psi and $C_{c=5.55\text{mil}}$=0.129 GPM/psi. Compare these magnitudes against the measured values, C~0.453 GPM/psi for the large clearance damper

and C~0.084 GPM/psi for the small clearance damper. Hence, simple theory predicts a larger flow conductance (lesser flow resistance) than the measurements evidence. Clearly the difference is attributed to the flow resistance in the central groove and the uneven pressure distribution since there are three supply holes. Note that for both dampers, the ratio C_{test}/C_{theory}~0.65.

Even when adding the groove ½ axial length in Eq. (9), i.e., with L=1.25 in, the predictions render a slight decrease in flow conductance and C_{test}/C_{theory}~0.78. Thus, the measured flow conductances, lesser than simple theory predicts, are due to the flow interactions in the central groove.

Using a computational model that accounts for the central groove and feed holes [9], the PI conducted a parametric study on effective groove depths to match the recorded flow rates and thus obtaining identical flow conductances. The analysis requires of an effective groove depth d_η=1.6c [6] to predict similar flow conductances, i.e., C~0.452 GPM/psi for the large clearance damper, and C~0.080 GPM/psi for the small clearance damper.

The required effective groove depths, a little deeper than the actual film clearance, demonstrate that the feed groove has a significant flow resistance; in direct opposition to the common assumption of a flow source (negligible flow resistance). For reference, Figure 11 shows the predicted static pressure field for a centered damper with the small clearance. Note that the pressure in the groove section varies circumferentially from one feed hole to the next. In the film land, the pressure drops linearly towards the ambient condition; however, the upstream condition at the interface with the edge of the central groove is largely affected by the holes disposition and effective groove depth.

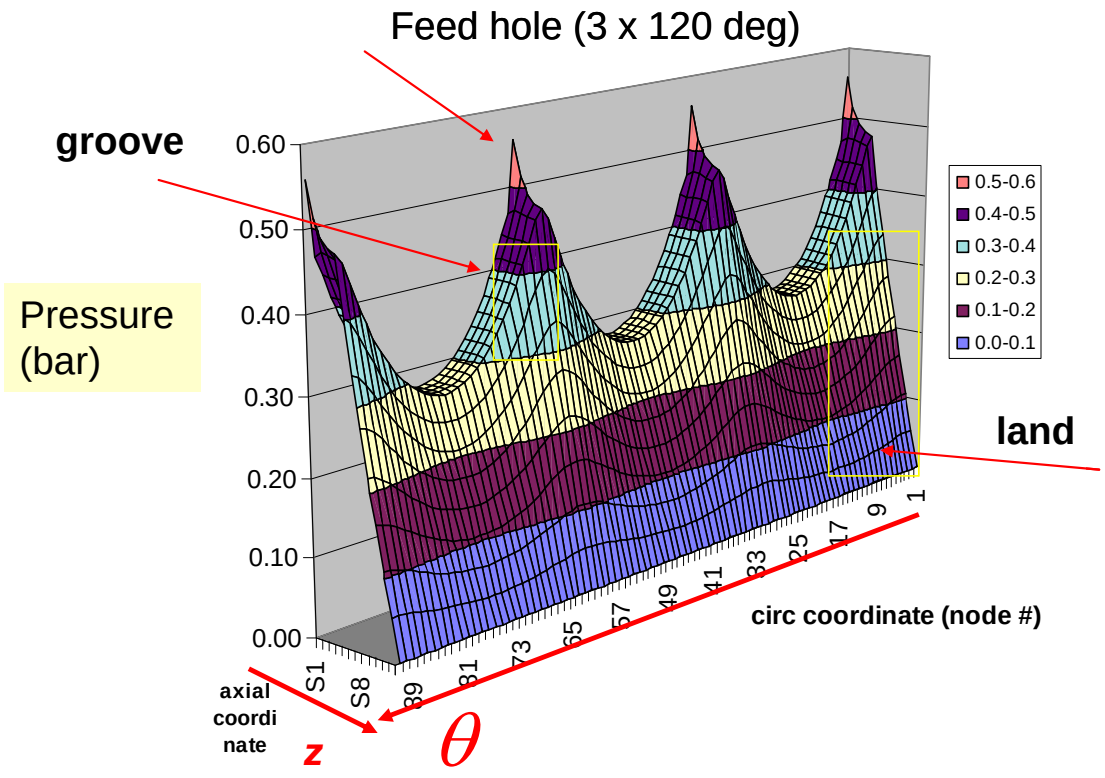

Fig. 11. Open ends SFDs: Predicted pressure field for damper with one inch film land lengths and clearance clearances *c*~5.5 mil. Supply pressure 8.10 psi (0.55 bar).

Predictions of SFD force coefficients and comparisons to test data

San Andrés and Delgado [5,6] advance a sound physical bulk-flow model for prediction of the pressure film in thin film land sections separated by grooves, as shown in Fig. 12. The model bridges the gap between extensive experimental data[1] in oil seal rings and SFDs and simple model predictions that ignore the flow field in grooved regions. The finite element analysis solves numerically the modified Reynolds equation

$$\frac{\partial}{R\partial\Theta}\left(h^3\frac{\partial P}{R\partial\Theta}\right)+\frac{\partial}{\partial z}\left(h^3\frac{\partial P}{\partial z}\right)=12\,\mu\frac{\partial h}{\partial t}+\rho h^2\,\frac{\partial^2 h}{\partial t^2} \qquad (9)$$

[1] The test data shows force coefficients much larger than classical model predictions; thus the need for a more accurate development. Please see Refs. [5,6] for a comprehensive review of the literature, the foundation of the model, and comparisons of predictions to archival test data. In 2012, the ASME –IGTI Structures and Dynamics Division gave a Best Paper Award to Ref. [6].

where h and P are the fluid film thickness and film pressure in the lubricated flow region $\{0 \le \Theta \le 2\pi, 0 \le z \le L + \frac{1}{2} L_G\}$. Above μ and ρ are the lubricant viscosity and density, respectively. The modified Reynolds equation above accounts for temporal fluid inertia effects. The film thickness is

$$h_{(\Theta,z,t)} = c_{(z)} + e_{X_{(t)}} \cos(\Theta) + e_{Y_{(t)}} \sin(\Theta) \tag{10}$$

where $c_{(z)}$ is a step-wise clearance distribution along the axial direction and (e_X, e_Y) are the components of the instantaneous journal center eccentricity.

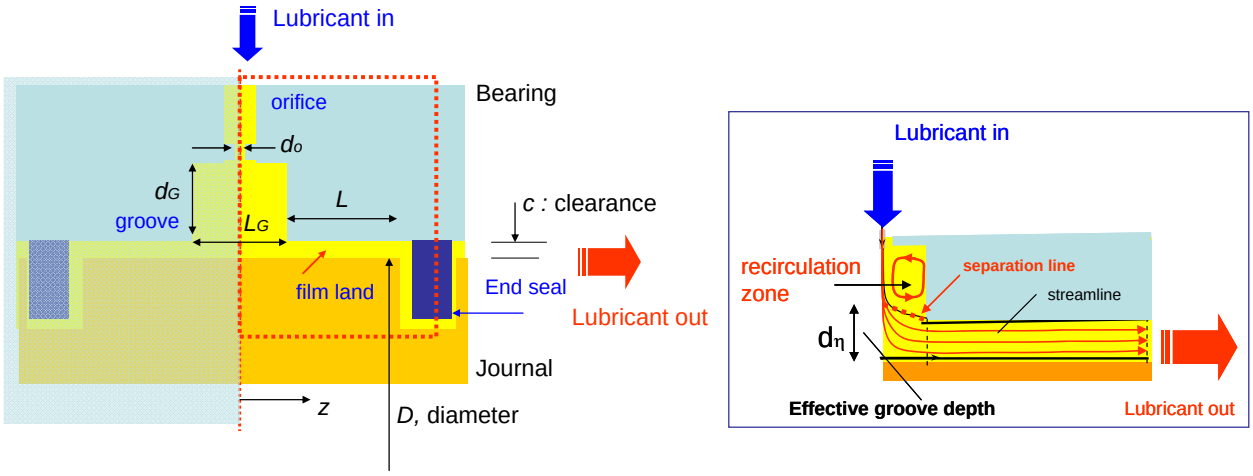

Fig. 12. Geometry and nomenclature for a model SFD with a central groove. Inset shows effective groove depth [6].

As per Refs. [5,6], a groove effective depth (d_η) lesser than the physical depth (d_G) is needed to predict accurately SFD force coefficients. Presently, as depicted in Fig. 12, the effective depth d_η=1.6c (8.88 mil and 15.84 mil) for both dampers is based on a close matching of the predicted flow rate to the measured flow magnitudes.

Recall the experimental force coefficients are derived from small amplitude (r=0.5 mil) circular orbits about a static eccentricity (e_S), 45° away from the X, Y axes. Presently, predictions are obtained for perturbations of the journal center about the equilibrium position. Figure 13 shows a comparisons of the current predictions for direct damping and inertia force coefficients and the experimental force coefficients (see Fig. 7) versus static eccentricity for the dampers with a small and large clearances, c=5.55 mil and c=9.9 mil. The graphs also display the theoretical force coefficients based on the classical lubrication equations, See Eqs. (6).

The comparisons show that the current computational model [10] does a good job in predicting accurate force coefficients. Notice the large difference between the current predictions and test data and the magnitudes predicted by the simple classical lubrication formulas. The discrepancies are due to the flow interaction in the central groove and which generate a large dynamic pressure field.

The model predicts for the large clearance damper: larger inertia coefficients and lesser damping coefficients than the test values. On the other hand, for the small clearance SFD, the model predicts more damping and less inertia coefficients than the experimental results. The discrepancies may be due to the constant value of effective groove depth selected for the analysis and also because the effect of the feed holes is not properly accounted for when the damper describes circular orbits.

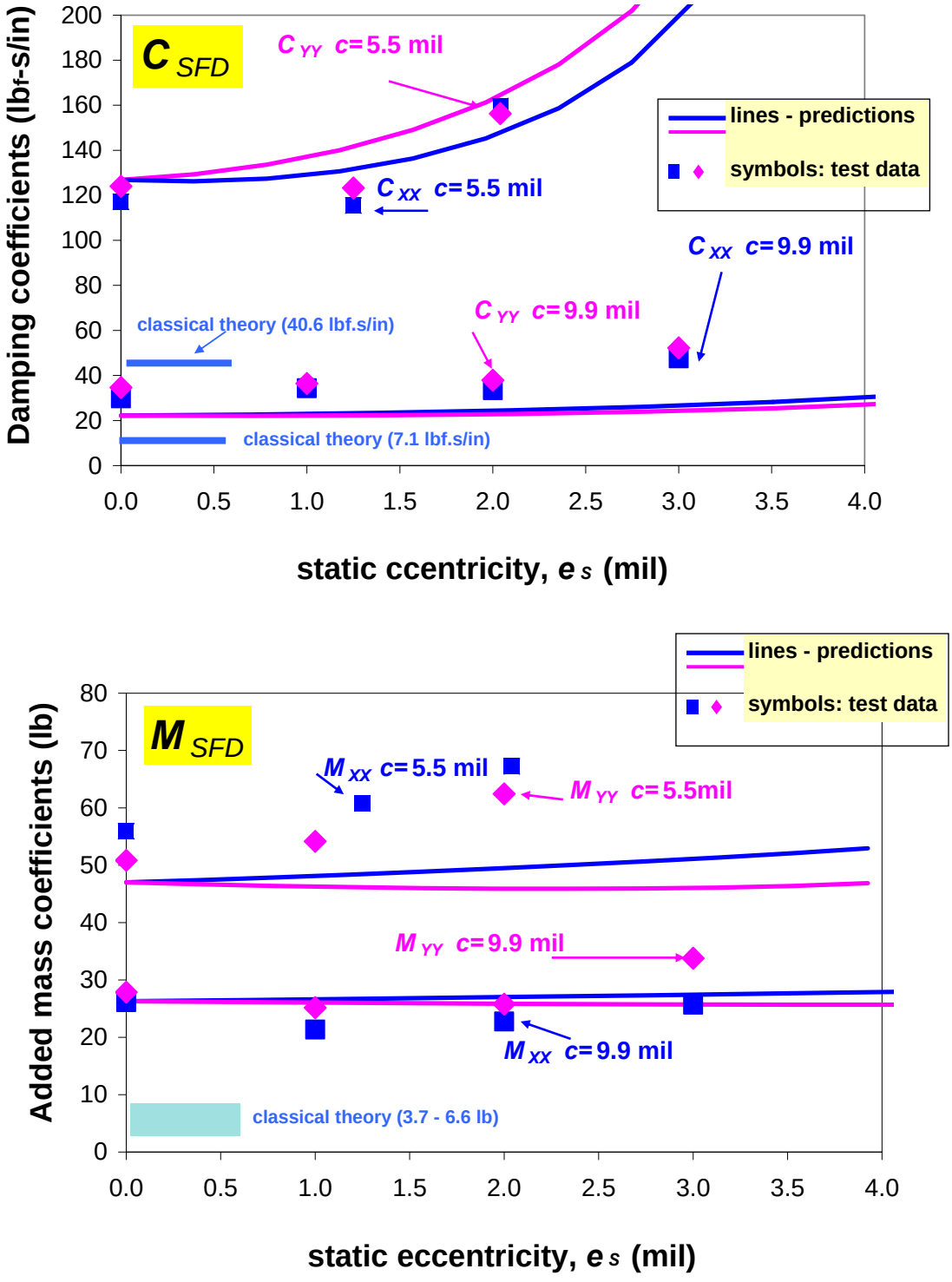

Fig. 13. Comparison of predicted and measured damping (C_{XX}, C_{YY})$_{SFD}$ and inertia (M_{XX}, M_{YY})$_{SFD}$ coefficients versus static eccentricity (e_S). Open ends SFDs: radial clearances c~5.5 mil and 9.9 mil. Orbit radius amplitude r=0.5 mil. Predictions obtained with effective groove depth d_η=1.6c

Conclusions

Note: The project received funding in December 2011, effectively starting on January 1, 2012.

The report describes the components and operation of a large load SFD test rig, details measurements of dynamic loads conducted on a large clearance (c=9.9 mil) open ends, centrally grooved SFD, and presents the experimental SFD force coefficients for operation at three static eccentric positions. The damper consists of two parallel film lands, one inch in length, separated by a deep central groove, ½ inch in width. Three equally spaced holes, 120° apart, supply an ISO VG 2 lubricant into the central groove at room temperature.

The experimental SFD force coefficients are compared to test results obtained earlier with the same damper but with a smaller clearance (c=5.5 mil) [3] and against predictions obtained from an advanced physical model that includes the flow field in the central groove and the interaction with the adjacent film lands [10]. Dynamic pressures recorded in the film lands (top and bottom) and in the central groove reveal that the central groove does not isolate the adjacent film lands but actually is a region where dynamic pressures are as large as in the film lands. This phenomenon is presently the rule rather than the exception as abundant test data in the laboratory and practice attest [5-7].

The measurements show negligible cross-coupled force coefficients since the orbital motions are of small amplitude (r=0.5 mil ~ 0.05c) albeit the excitation frequencies are as large as 250 Hz and with large amplitude dynamic forces (~ 90 lb_f).

The experimental squeeze films damping and stiffness coefficients are much larger than predictions obtained from classical lubrication theory [2]. For example, at the centered ($\underline{e_s}$=0) and largest static eccentricity ($\underline{e_s}$=3 mil), the force coefficients extracted from the dynamic load measurements, the advanced predictive model [10], and those based on classical lubrication are listed below:

Centered bearing	K_{XX} (klb_f/in)	K_{YY} (klb_f/in)	M_{XX} (lb)	M_{YY} (lb)	C_{XX} (lb_f-s/in)	M_{YY} (lb_f-s/in)
Experimental	**-1.6**	**-1.4**	**27.4**	**29.8**	**30.3**	**34.7**
Perturbation analysis [10]	**0.00**	**0.00**	**22.2**	**22.2**	**26.3**	**26.3**
Orbital analysis, App C	**0.07**	**0.07**	**22.2**	**22.2**	**26.3**	**26.3**
Classical Lubrication, Eqs. (6)	**0.0**	**0.0**	**3.19**	**3.19**	**7.16**	**7.16**

Off-centered 3 mil	K_{XX} (klb_f/in)	K_{YY} (klb_f/in)	M_{XX} (lb)	M_{YY} (lb)	C_{XX} (lb_f-s/in)	M_{YY} (lb_f-s/in)
Experimental	**-1.6**	**-1.4**	**27.4**	**29.8**	**30.3**	**34.7**
Perturbation analysis [10]	**0.060**	**0.071**	**25.7**	**27.7**	**25.4**	**28.2**
Orbital analysis, App C	**0.061**	**0.071**	**25.8**	**27.5**	**24.3**	**26.7**
Classical Lubrication, Eqs. (6)			**NA**	**NA**		

Hence, the open ends centrally grooved damper delivers ~3.5 times more damping than the classical formula predicts and generates a ~7.4 larger added mass. The measurements thus reveal the limited applicability of the classical formulas and make pathetic the need to use a more advanced model to predict accurately the dynamic forced of SFDs in practice.

The experimental force coefficients for the large clearance damper are also compared against prior experimental results for an identical damper (diameter and length) but with a smaller clearance, c=5.5 mil [3]. The experimental results show the added masses scale well with ($1/c$); however, the damping force coefficients are not proportional to $1/c^3$. The ratio of damping force coefficients for the small and large clearance dampers is ~3.80 while the scale law ($1/c^3$) gives 5.68. The discrepancy is due to the generation of an uneven static pressure field in the groove region as determined by the disposition of the lubricant feed holes.

Appendix C details the orbital analysis model implemented in an updated version of the computational model described in Ref. [10]. The novel analysis will deliver more accurate force coefficients representative of actual SFD orbital paths.

Nomenclature

$\mathbf{a}_{(t)}$	$\{a_X, a_Y\}^T$ Vector of bearing accelerations [m/s^2]
$\bar{\mathbf{a}}_{(\omega)}$	$DFT\left[\mathbf{a}_{(t)}\right]$ Discrete Fourier transform of accelerations [m/s^2]
c	Film land clearance [m]
C	Damping coefficient [N.s/m]
C_c	$Q/\Delta P$. Flow conductance [LPM/Pa]
d_G	Groove depth [m]
d_η	Effective groove depth [m]
D	Journal diameter [m], R= ½ D
e_S	Static eccentricity (along 45^o) [m]
e_X, e_Y	Dynamic eccentricity components [m]
f_n	Natural frequency [rad/s]
$\mathbf{F}_{(t)}$	$\{F_X, F_Y\}^T$ Vector of dynamic loads [N]
$\bar{\mathbf{F}}_{(\omega)}$	$DFT\left[\mathbf{F}_{(t)}\right]$ Discrete Fourier transform of accelerations [m/s^2]
$\mathbf{G}$	$\mathbf{H}^{-1}$. Flexibility matrix [m/N]
$\mathbf{H}$	$\mathbf{K} - \omega^2\mathbf{M} + i\,\omega\mathbf{C}$. Matrix of impedance coefficients [N/m]
i	$\sqrt{-1}$. Imaginary unit
K	Stiffness coefficient [N/m]
K_S	Support stiffness [N/m]
M	Mass coefficient [kg]
M_{BC}	Bearing cartridge mass [kg]
L	Film land length [m]
L_G	Grove width [m]
Q_{in}	Flow rate [LPM]
Q_b	Flow rate through bottom land [LPM]
P	Film pressure [Pa]
P_G	Static oil pressure in central groove [Pa]
P_l, P_g	Dynamic pressures in film land and central groove [Pa]
r	Circular orbit amplitude [m]
t	Time [s]
X,Y	Coordinate axes
$\mathbf{z}_{(t)}$	$\{x,y\}^T$ Vector of bearing displacements relative to journal [m]
$\bar{\mathbf{z}}_{(\omega)}$	$DFT\left[\mathbf{z}_{(t)}\right]$ Discrete Fourier transform of bearing displacements [m]
ξ	Damping ratio [-]
θ	x/R. Circumferential coordinate [rad]
ρ,μ	Oil density [kg/m^3] and viscosity [Pa.s]
ω	Excitation frequency [rad/s]

Subscripts

s	Structure
LUB	Lubricated system
SFD	Squeeze film damper

References

[1] Zeidan, F., San Andrés, L., and Vance, J.M., 1996, "Design and Application of Squeeze Film Dampers in Rotating Machinery," Proc. of the 25th Turbomachinery Symposium, Turbomachinery Laboratory, Texas A&M University, pp. 169-188, September, Houston.

[2] San Andrés, L., 2010, "Squeeze Film Dampers: Operation, Models and Technical Issues," Modern Lubrication Theory, Notes 13, Texas A&M University Digital Libraries, https://repository.tamu.edu/handle/1969.1/93197

[3] Seshaghiri, S., 2011, "Identification of Force Coefficients in Two Squeeze Film Dampers with a Central Groove," M.S. Thesis, Texas A&M Univ., College Station, TX., USA.

[4] Mahecha, P., 2011, "Experimental Dynamic Forced Performance of a Centrally Grooved, End Sealed Squeeze Film Damper," M.S. Thesis, Texas A&M Univ., College Station, TX., USA.

[5] Delgado, A., and San Andrés, L., 2010, "A Model for Improved Prediction of Force Coefficients in Grooved Squeeze Film Dampers and Grooved Oil Seal Rings", ASME Journal of Tribology, **132**(July), p. **032202** (1-12)

[6] San Andrés, L., and Delgado, A., 2012, "A Novel Bulk-Flow Model for Improved Predictions of Force Coefficients in Grooved Oil Seals Operating Eccentrically," ASME J. Eng. Gas Turbines Power, **134**(May), p. **052509** (1-10)

[7] San Andrés, L., 2012, "Damping And Inertia Coefficients for Two Open Ends Squeeze Film Dampers with a Central Groove: Measurements and Predictions," ASME Paper GT2012-6212 (accepted for publication at ASME J. Eng. Gas Turbines Power)

[8] San Andrés, L., 2009, *Modern Lubrication Theory,* "Experimental Identification of Bearing Force Coefficients," Notes 14, Texas A & M University Digital Libraries, http://repository.tamu.edu/handle/1969.1/93197

[10] San Andrés, L., 2010, "PW_SFD_2010," SFD Predictive Code Developed for Pratt & Whitney Engines, MEEN Dept., Texas A&M University**,** Proprietary

Appendix A. Sample of flexibility and impedance functions for lubricated test system

(a) Tests at centered condition, e_S= 0 mil

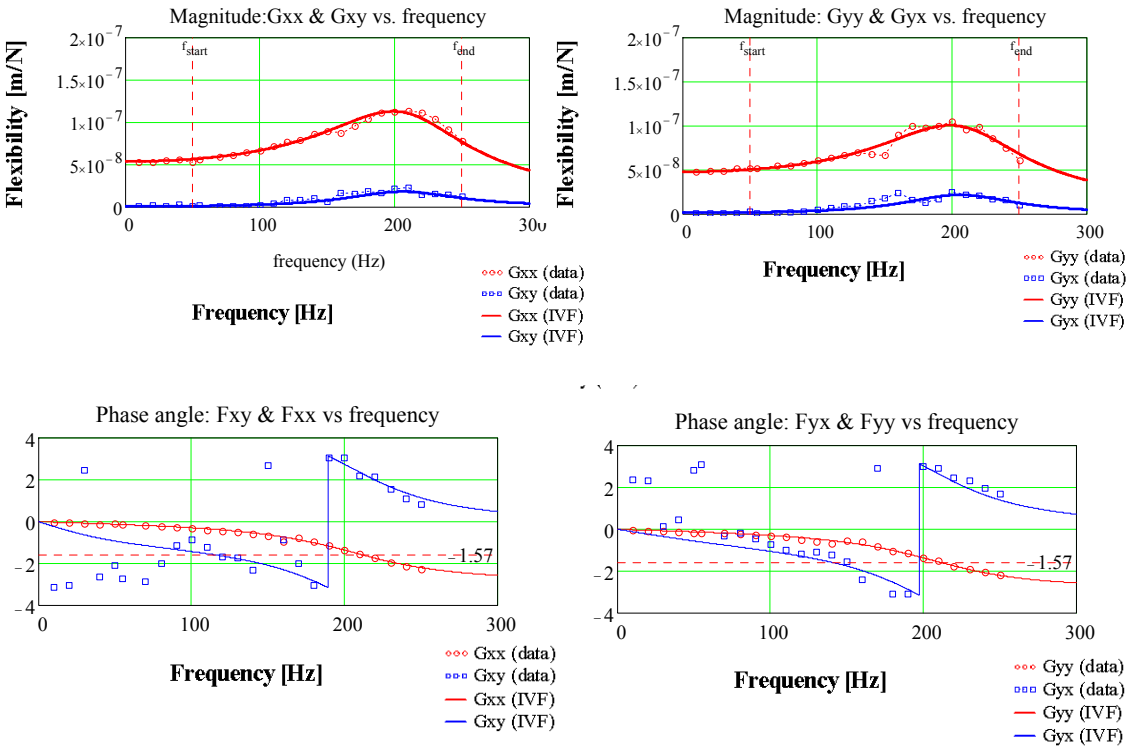

Fig. A1 Amplitude and phase angle of flexibility functions G_{ij} vs. excitation frequency for lubricated test system. Experimental values and model curve fits. Identification range 120 – 230 Hz. Open ends damper with *c*=10mil and one inch land lengths. Centered journal (e_S=0 mil), circular orbits *r* =0.5 mil.

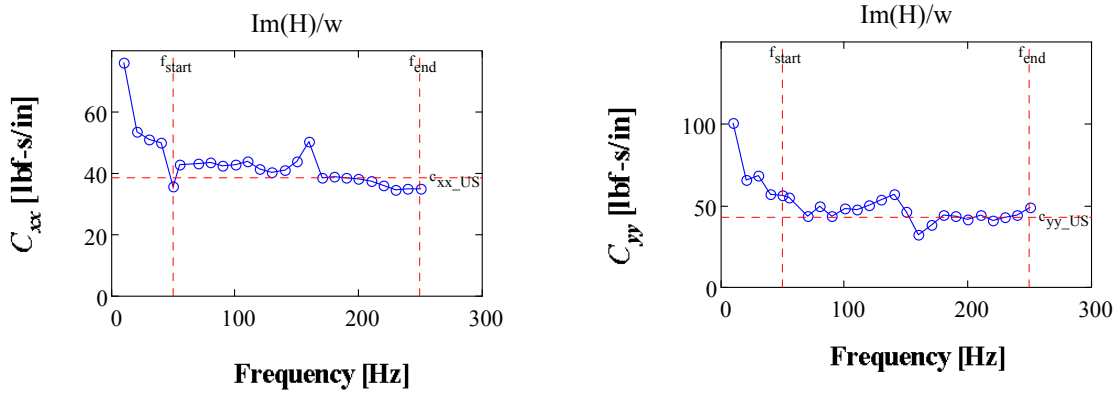

Fig. A2 Estimated damping coefficients (C_{XX}, C_{YY}) and Im(H)/ω vs. excitation frequency for open ends damper with *c*=10mil and one inch land lengths. Centered journal (e_S=0 mil), circular orbits *r* =0.5 mil.

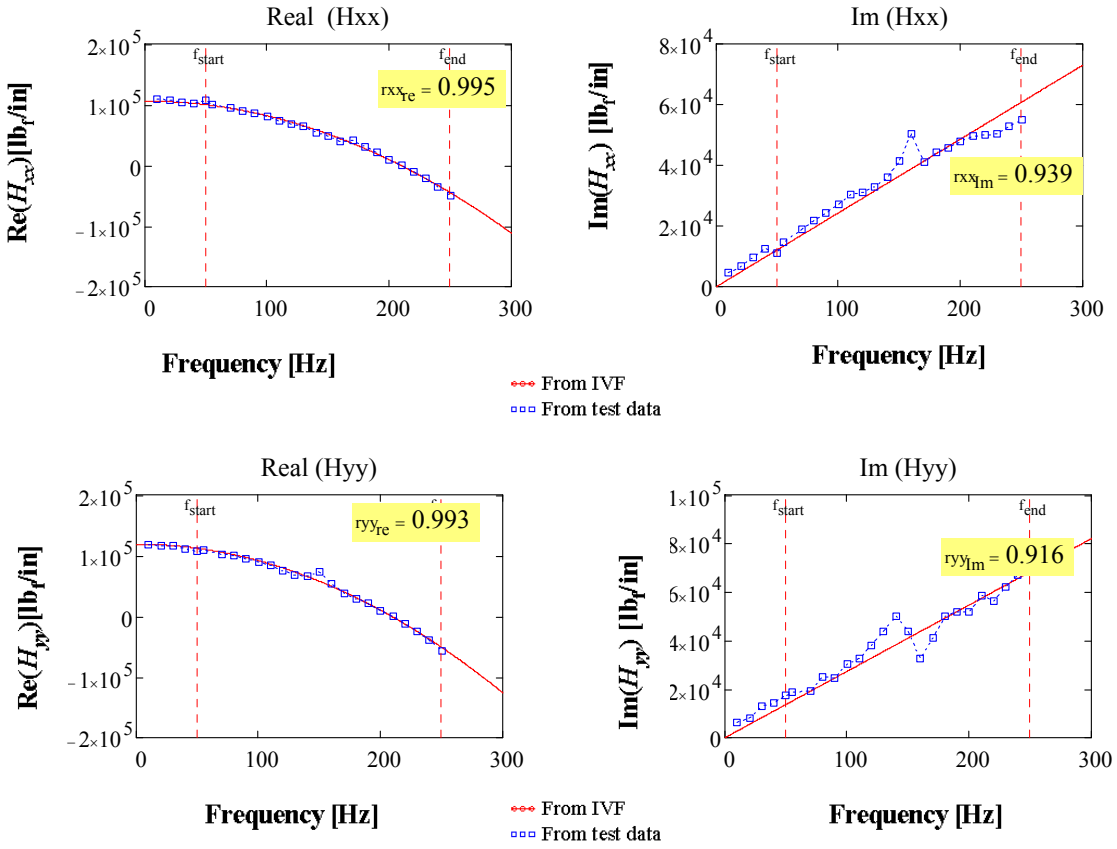

Fig. A3 Real and imaginary parts of direct impedances (H_{XX} , H_{YY}) vs. excitation frequency. Experimental data and fits using identified parameters. Open ends damper with *c*=10mil and one inch land lengths. Centered journal (e_S=0 mil), circular orbits *r* =0.5 mil.

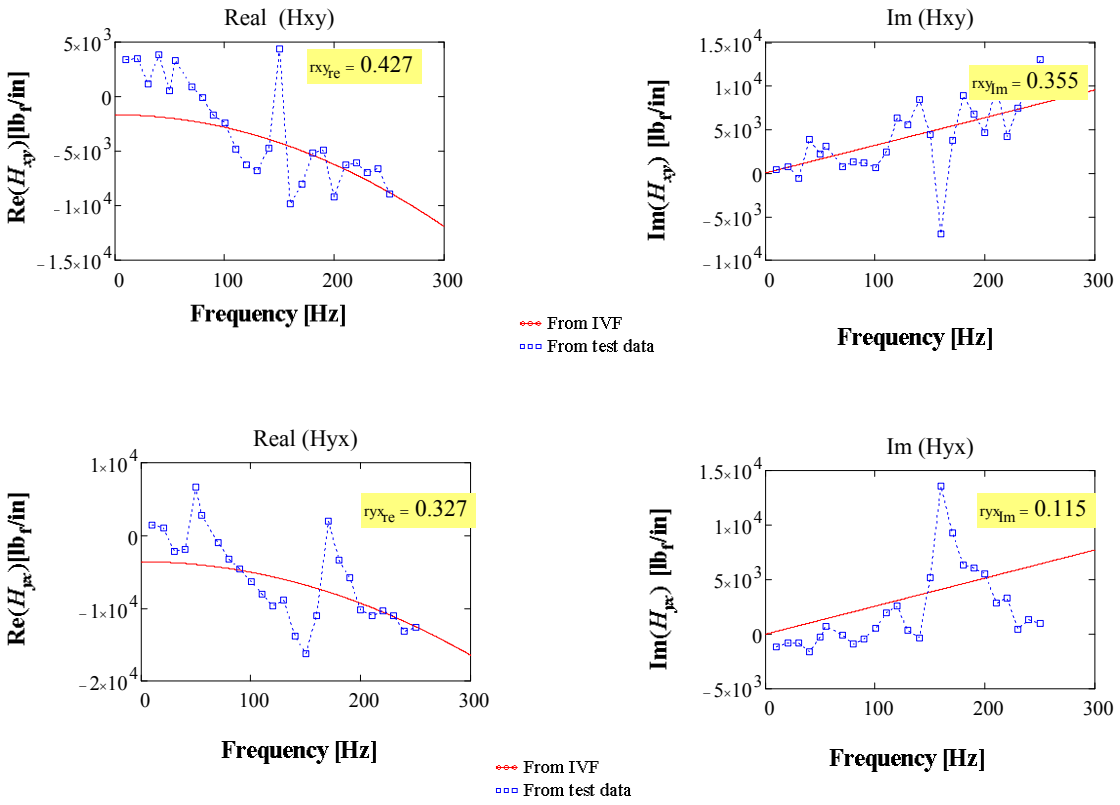

Fig. A4. Real and imaginary parts of cross impedances (H_{XY} , H_{YX}) vs. excitation frequency. Experimental data and fits using identified parameters. Open ends damper with c=10mil and one inch land lengths. Centered journal (e_S=0 mil), circular orbits r =0.5 mil.

(b) Tests at off-centered displacement e_S= 3 mil

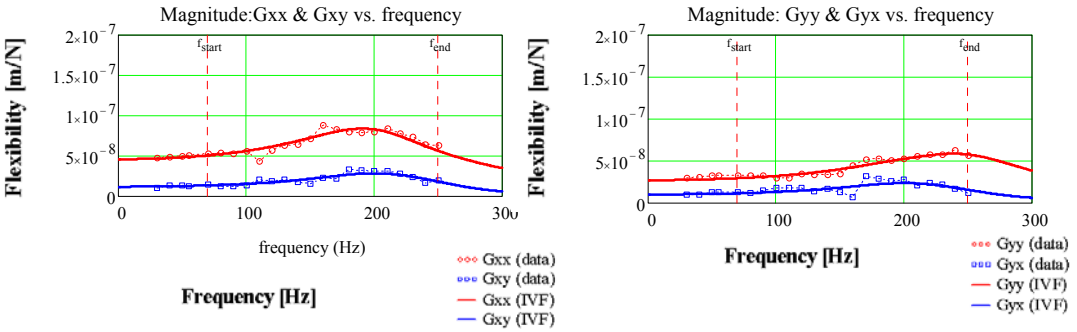

Fig. A5 Amplitude of flexibility functions G_{ij} vs. excitation frequency for lubricated test system. Experimental values and model curve fits. Identification range 120 – 230 Hz. Open ends damper with c=10mil and one inch land lengths. Off-centered journal (e_S=3 mil), circular orbits r =0.5 mil.

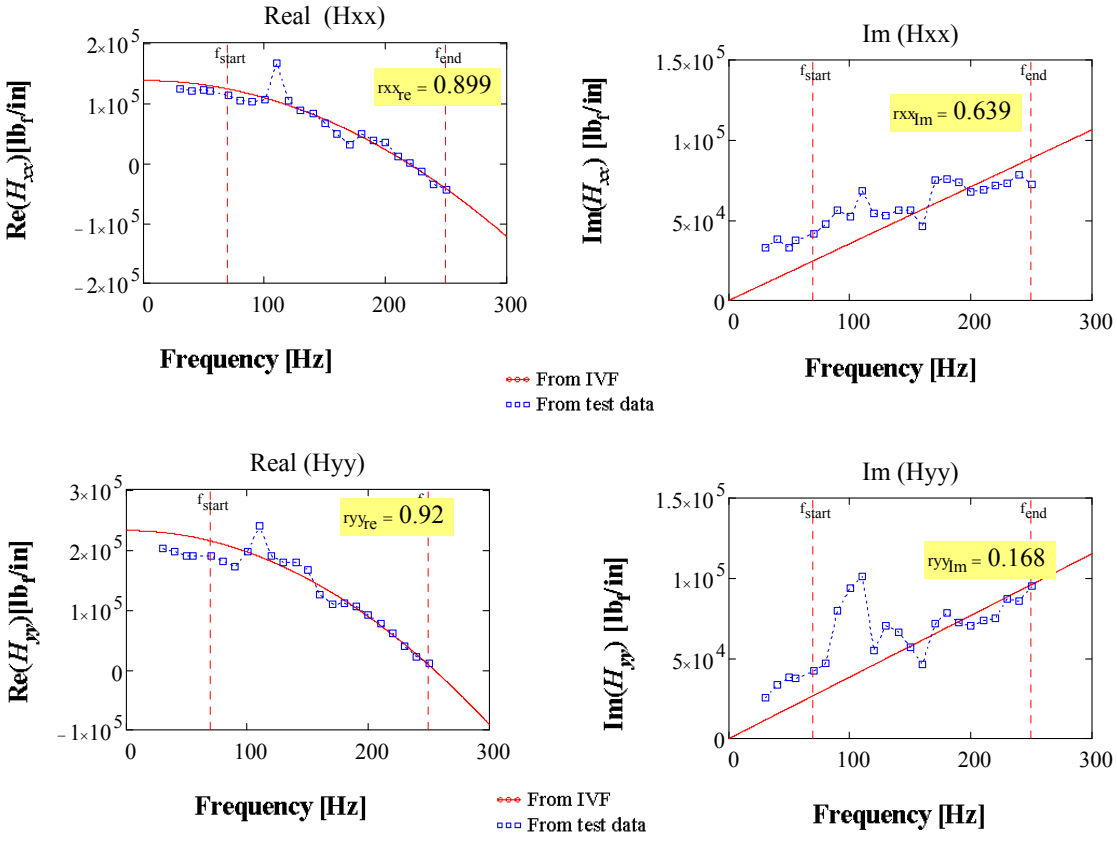

Fig. A6 Real and imaginary parts of direct impedances (H_{XX} , H_{YY}) vs. excitation frequency. Experimental data and fits using identified parameters. Open ends damper with c=10mil and one inch land lengths. Off-centered journal (e_S=3 mil), circular orbits r =0.5 mil.

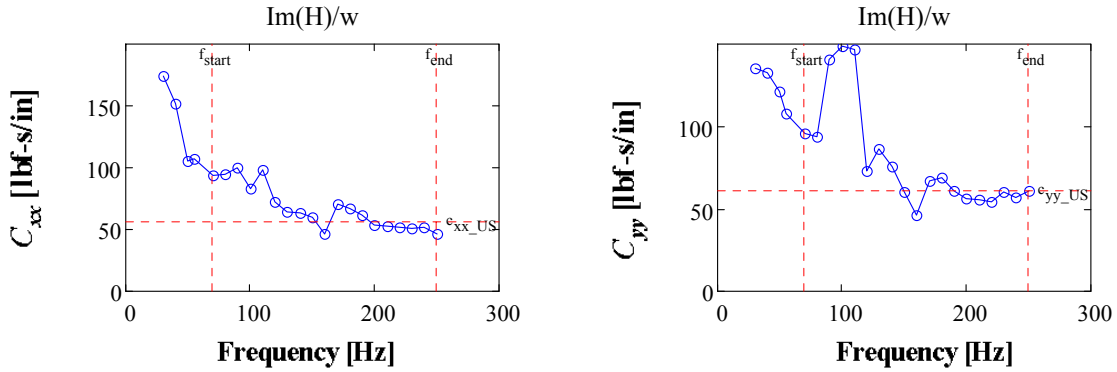

Fig. A7. Estimated damping coefficients (C_{XX}, C_{YY}) and Im(H)/ω vs. excitation frequency for open ends damper with *c*=10mil and one inch land lengths. Off-centered journal (e_S=3 mil), circular orbits *r* =0.5 mil.

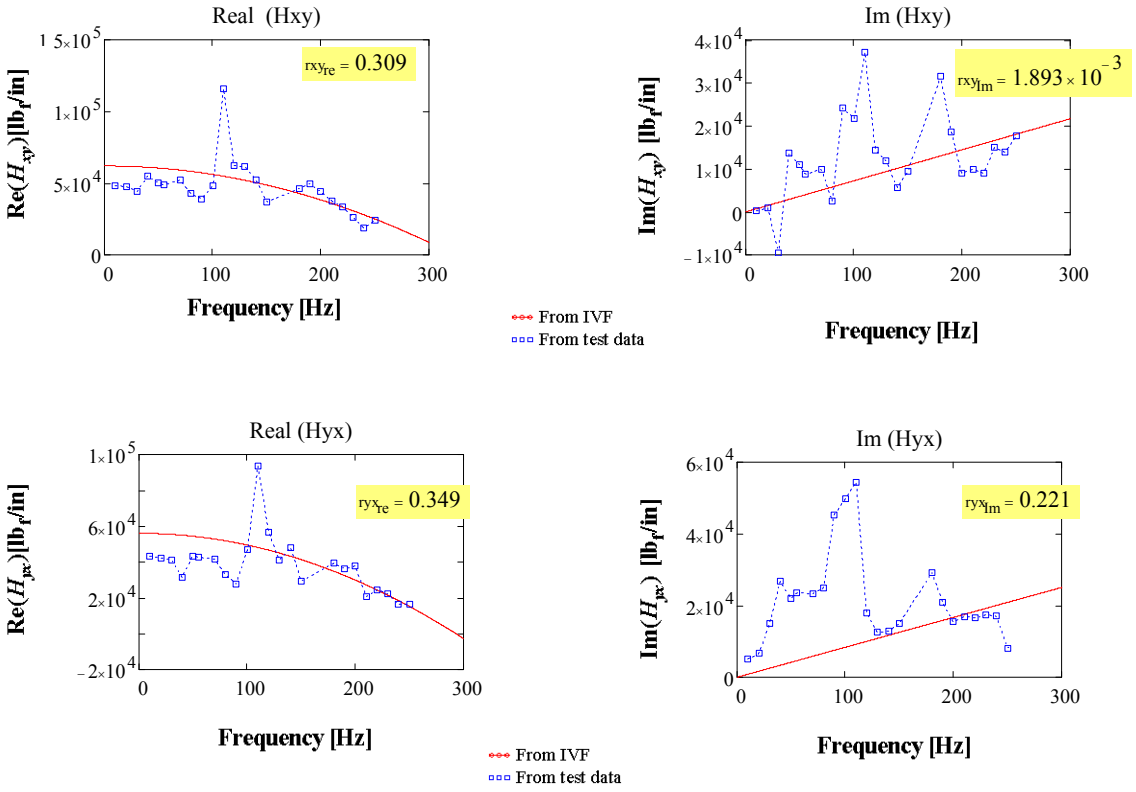

Fig. A8 Real and imaginary parts of cross impedances (H_{XY} , H_{YX}) vs. excitation frequency. Experimental data and fits using identified parameters. Open ends damper with *c*=10mil and one inch land lengths. Off-centered journal (e_S=3 mil), circular orbits *r* =0.5 mil.

Appendix B. Uncertainty and goodness of fit for estimated force coefficients

Table B.1 list the uncertainties for the identified physical parameters (stiffness, damping and inertia) and the goodness of fit with the physical (*K-C-M*) model. This table complements the identified force coefficients in Table 4, pg. 12. Refs. [3,4] give details on the uncertainty analysis.

In general the uncertainties for all the parameters are a small fraction (5% or less) of the magnitude reported. For the tests with BC static eccentricity e_S= 0, 1 and 2 mil, the goodness of fit, R^2~0.95 and higher, denotes the physical parameters $(K, C, M)_{XX,YY}$ represent very well the experimentally derived impedances. On the other hand for the case e_S=3 mil, the goodness of fit are too low thus indicating the physical model does not represent the experimental data with any accuracy.

Table B1. Open ends SFD lubricated test system: Uncertainty and goodness of fit for force coefficients. From tests at various BC eccentric positions (e_S=1, 2 and 3 mil). Circular orbits with amplitude *r*=0.5 mil, frequency range 50 – 250 Hz. Film land clearance *c*=9.9 mil and one inch land lengths

Static eccentricity (mil)	Direct coefficients						Goodness of fit			
	U_{KXX} (klbf/in)	U_{KYY} (klbf/in)	U_{MXX} (lb)	U_{MYY} (lb)	U_{CXX} (lbf-s/in)	U_{CYY} (lbf-s/in)	Re (*XX*)	Re (*YY*)	Im (*XX*)	Im (*YY*)
0.0	1.7	1.9	0.7	0.8	0.8	0.9	0.995	0.993	0.939	0.916
1.0	1.7	1.9	0.7	0.7	0.9	1.0	0.889	0.977	0.637	0.823
2.0	1.6	1.8	0.7	0.8	0.9	1.0	0.987	0.993	0.969	0.960
3.0	2.1	3.6	0.8	1.0	1.2	1.2	0.899	0.920	0.639	0.168

Static eccentricity (mil)	Cross coupled coefficients						Goodness of fit			
	U_{KXY} (klbf/in)	U_{KYX} (klbf/in)	U_{MXY} (lb)	U_{MYX} (lb)	U_{CXY} (lbf-s/in)	U_{CYX} (lbf-s/in)	Re (*XY*)	Re (*YX*)	Im (*XY*)	Im (*YX*)
0.0	0	-0.1	0	0	0.4	0.4	0.427	0.327	0.355	0.115
1.0	0	-0.1	0	0	0.4	0.4	0.112	0.018	0.066	0.018
2.0	0	0	0	0.1	0.4	0.4	0.411	0.340	0.344	0.302
3.0	0.9	0.8	0.2	0.2	0.5	0.5	0.306	0.283	0.003	0.237

Appendix C. Estimation of bearing force coefficients from orbital paths

Fluid film bearing analytical models and computational programs predict rotordynamic force coefficients for a specified static equilibrium eccentricity (see inset). The mechanical parameters, hereby labeled as the true (linear) force coefficients, represent the idealization of infinitesimally small amplitude journal motions about an static position or equilibrium eccentricity (x_e, y_e).

Fluid film bearing reaction forces $\mathbf{F}=\{F_X,\ F_Y\}^{\mathrm{T}}$ relate to journal center motions $\Delta x = \left(x_{(t)} - x_e\right), \Delta y = \left(y_{(t)} - x_e\right)$ by

$$\begin{Bmatrix} F_X \\ F_Y \end{Bmatrix} = \begin{Bmatrix} F_{X_e} \\ F_{Y_e} \end{Bmatrix} - \begin{bmatrix} K_{XX} & K_{XY} \\ K_{YX} & K_{YY} \end{bmatrix} \begin{Bmatrix} x \\ y \end{Bmatrix} - \begin{bmatrix} C_{XX} & C_{XY} \\ C_{YX} & C_{YY} \end{bmatrix} \begin{Bmatrix} \dot{x} \\ \dot{y} \end{Bmatrix} - \begin{bmatrix} M_{XX} & M_{XY} \\ M_{YX} & M_{YY} \end{bmatrix} \begin{Bmatrix} \ddot{x} \\ \ddot{y} \end{Bmatrix} \qquad \text{(C.1)}$$

or

$$\mathbf{F}_{(t)} = \mathbf{F}_e - \mathbf{K}\,\Delta\mathbf{z} - \mathbf{C}\,\Delta\dot{\mathbf{z}} - \mathbf{M}\,\Delta\ddot{\mathbf{z}} \qquad \text{(C.2)}$$

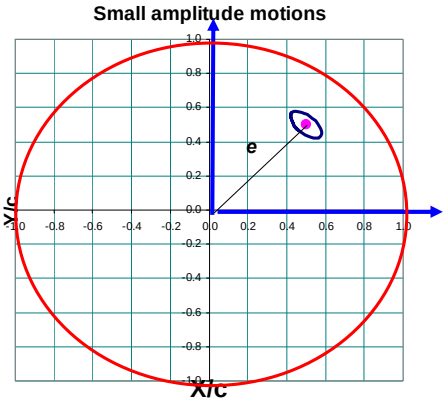

where $\mathbf{F_e}$ is the bearing static reaction force vector at the equilibrium position (x_e, y_e). Above, the matrices **K, C** and **M** contain the stiffness, damping and inertia force coefficients, respectively. Fluid inertia or added coefficients (**M**) are significant in squeeze film dampers and seals with dense fluids operating at high speeds and with large pressure differentials. In general, the force coefficients for liquid (incompressible fluid) bearings or seals are frequency independent; thus, the physical **K-C-M** model is quite adequate. However, bearings or seals handling compressible fluids (gases) show force coefficients that depend strongly on the frequency (ω) of whirl motion; hence, $\mathbf{K}=\mathbf{K}_{(\omega)}$ and $\mathbf{C}=\mathbf{C}_{(\omega)}$. Incidentally, bearings with compliant surfaces or moving parts, such as tilting pad bearings, also show strong frequency effects in their dynamic forced response.

Recall that the (linear) force coefficients represent changes in bearing reaction forces to small amplitude motions about an equilibrium position; that is

$$K_{XY} = -\left.\frac{\partial F_X}{\partial y}\right|_{(x_e, y_e)} ; C_{YX} = -\left.\frac{\partial F_Y}{\partial \dot{x}}\right|_{(x_e, y_e)} ; M_{XX} = -\left.\frac{\partial F_X}{\partial \ddot{x}}\right|_{(x_e, y_e)} \qquad \text{(C.3)}$$

for example. The mathematical formulation calls for infinitesimally small motions; however, engineering use and practice show these coefficients to be valid in producing bearing reaction forces with journal whirl motions of sizable amplitudes. Often, the applicability of a theoretical formulation goes well beyond rigorous mathematical definitions.

The archival literature, every so often, presents studies[2] that question the validity of the linearized force representation, Eq. (C.1), and embark on non-linear analyses to assess (quantify) the error in using the linearized formulation as opposed to a *"more exact"* model derived from a Taylor-series expansion of the forces; say,

$$\begin{aligned} F_{X_{(t)}} = F_{X_e} &+ \left[\left.\frac{\partial F_X}{\partial x}\right|_e \Delta x + \frac{1}{2!}\left.\frac{\partial^2 F_X}{\partial x^2}\right|_e \Delta x^2 + \frac{1}{3!}\left.\frac{\partial^3 F_X}{\partial x^3}\right|_e \Delta x^3 + ... \right] \\ &+ \left[\left.\frac{\partial F_X}{\partial y}\right|_e \Delta y + \frac{1}{2!}\left.\frac{\partial^2 F_X}{\partial y^2}\right|_e \Delta y^2 + \frac{1}{3!}\left.\frac{\partial^3 F_X}{\partial y^3}\right|_e \Delta y^3 + ... \right] + \left[\left.\frac{\partial^2 F_X}{\partial x \partial y}\right|_e \Delta x \Delta y + ... \right] \\ &+ \left[\left.\frac{\partial F_X}{\partial \dot{x}}\right|_e \Delta \dot{x} + \frac{1}{2!}\left.\frac{\partial^2 F_X}{\partial \dot{x}^2}\right|_e \Delta \dot{x}^2 + \frac{1}{3!}\left.\frac{\partial^3 F_X}{\partial \dot{x}^3}\right|_e \Delta \dot{x}^3 + ... \right] \\ &+ \left[\left.\frac{\partial F_X}{\partial \dot{y}}\right|_e \Delta \dot{y} + \frac{1}{2!}\left.\frac{\partial^2 F_X}{\partial \dot{y}^2}\right|_e \Delta \dot{y}^2 + \frac{1}{3!}\left.\frac{\partial^3 F_X}{\partial \dot{y}^3}\right|_e \Delta \dot{y}^3 + ... \right] + \left[\left.\frac{\partial^2 F_X}{\partial \dot{x} \partial \dot{y}}\right|_e \Delta \dot{x} \Delta \dot{y} + ... \right] .... \end{aligned} \qquad \text{(C.4)}$$

which leads to both linear and nonlinear force coefficients. Clearly, the question is when to truncate the nonlinear model so as to keep its accuracy while ensuring some degree of computational efficiency. This question is perhaps irrelevant in an age of fast computing where engineering processes can readily integrate the complete nonlinear bearing model into a predictive environment and simply calculate at each time (step),

$$\begin{bmatrix} F_{X_{(t)}} \\ F_{Y_{(t)}} \end{bmatrix} = \mathbf{f}\left(x_{(t)}, y_{(t)}, \dot{x}, \dot{y}, \ddot{x}, \ddot{y}\right) \qquad \text{(C.5)}$$

[2] Tieu, A.K., and Qiu, Z.L., 1995, "Stability of Finite Journal Bearings–-from Linear and Nonlinear Bearing Forces," Trib. Trans., v. 38, pp. 627-635.
Braun, MJ, and Hu, Y., 1991, "Nonlinear Effects in a Plain Journal Bearing: Part 1—Analytical Study; Part 2—Results," ASME J. Tribol., 113, pp. 555–570.

SFDs often experience orbital (elliptical) motions with large amplitudes, thus violating the major assumption to derive linearized rotordynamic force coefficients. Presently, an existing computational model [10] also performs an orbit analysis to predict instantaneous reaction forces (F_X, F_Y) for a specified journal motion with arbitrary amplitudes of motion and static position. The model assumes single frequency (ω) motions[3] of the type

$$\begin{aligned} \bar{x}_{(t)} &= \bar{x}_S + \cos(\alpha)\,\bar{a}_{X(t)} - \sin(\alpha)\,\bar{a}_{Y(t)} \\ \bar{y}_{(t)} &= \bar{y}_S + \sin(\alpha)\,\bar{a}_{X(t)} + \cos(\alpha)\,\bar{a}_{Y(t)} \end{aligned} \qquad \text{(C.6)}$$

where $$\bar{a}_{X(t)} = \bar{r}_X \cos(\omega t + \phi),\ \bar{a}_{Y(t)} = \bar{r}_Y \sin(\omega t + \phi) \qquad \text{(C.7)}$$

Above $(\bar{x}_S, \bar{y}_S)$ denote the components of the static eccentricity vector, $(\bar{r}_X, \bar{r}_Y)$ are the amplitudes of motion along the X,Y axes, ϕ is a phase angle, and α is the angle of the ellipse axis with the X coordinate. Figure C.1 depicts a typical off-centered journal orbital motion with $(\bar{x}_S, \bar{y}_S)$=0.3c, $\bar{r}_X = 0.2c$, $\bar{r}_Y = 0.3c$, $\phi = 0$ and $\alpha = \frac{\pi}{4}$.

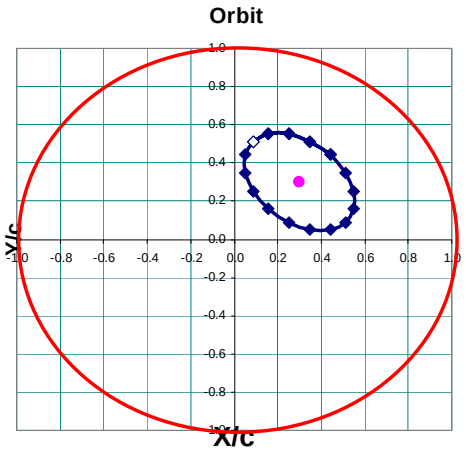

Fig. C.1 Example of journal describing off-centered, large amplitude elliptical motion

Figure C.2 depicts a typical example of an orbital analysis conducted with a large amplitude circular centered orbit. The motion path is specified and the damper reaction forces predicted at discrete points along the orbital path during a full period of whirl motion.

[3] The whirl frequency ω is positive, i.e. counter-clockwise as per the graph.

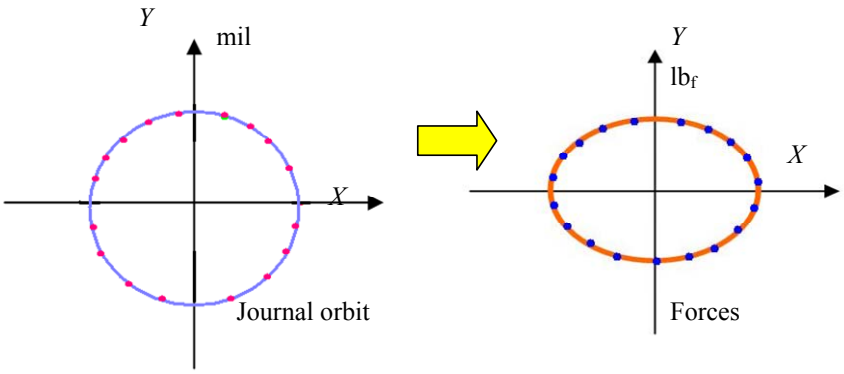

Fig. C.2 Example of circular centered orbit analysis: journal motion *X* vs *Y* and SFD reaction forces (F_X vs F_Y). Dots indicate discrete points at which code predicts SFD forces

The SFD instantaneous reaction force superimposes a dynamic force to a static force, i.e. $\mathbf{F}=\mathbf{F}_{\mathbf{static}}+\mathbf{F}_{\mathbf{dyn}}$. The dynamic component of the SFD reaction force is modeled in a linearized form as

$$\mathbf{F}_{\mathbf{dyn}} \approx \mathbf{K}_{\mathbf{SFD}}\,\mathbf{z} + \mathbf{C}_{\mathbf{SFD}}\,\dot{\mathbf{z}} + \mathbf{M}_{\mathbf{SFD}}\,\ddot{\mathbf{z}} \qquad \text{(C.8)}$$

where $\mathbf{z}$ is a vector of dynamic displacements and $(\mathbf{K},\ \mathbf{C},\ \mathbf{M})_{\mathbf{SFD}}$ are matrices of stiffness, viscous damping and inertia force coefficients. From Eq. (C.6), $\mathbf{z}$ is given by the real part of

$$\mathbf{z} = \left\{ \cos(\alpha) \begin{bmatrix} \bar{r}_X \\ -i\,\bar{r}_Y \end{bmatrix} + \sin(\alpha) \begin{bmatrix} i\,\bar{r}_Y \\ \bar{r}_X \end{bmatrix} \right\} e^{i(\omega t+\phi)} = \mathbf{z}_1 e^{i(\omega t+\phi)} \qquad \text{(C.9)}$$

where $\mathbf{z}_1 = \begin{bmatrix} x_c & y_c \end{bmatrix}^T$. The dynamic or time varying part of the reaction force is periodic with fundamental period $T=2\pi/\omega$. Using Fourier series decomposition, the damper dynamic reaction force $\mathbf{F}_{\mathbf{dyn}}$ can be decomposed as

$$\mathbf{F}_{\mathbf{dyn}} = \mathbf{F}_{\mathbf{I}} e^{i(\omega t+\phi)} + \mathbf{F}_{\mathbf{II}} e^{i(2\omega t+\phi)} + \mathbf{F}_{\mathbf{III}} e^{i(3\omega t+\phi)} + ... \qquad \text{(C.10)}$$

To satisfy Eq. (C.8), one must approximate the reaction force as

$$\mathbf{F}_{\mathbf{dyn}} \approx \mathbf{F}_{\mathbf{I}} e^{i(\omega t+\phi)} \qquad \text{(C.11)}$$

This approximation is valid for small amplitude motions and nearly centered operating conditions[4]. Substitution of Eqs. (C.11) and (C.9) into Eq. (C.8) gives

$$\mathbf{F}_1 \approx \left(\mathbf{K}_{\mathbf{SFD}} - \omega^2 \mathbf{M}_{\mathbf{SFD}} + i\,\omega \mathbf{C}_{\mathbf{SFD}}\right)\mathbf{z}_1 = \mathbf{H}\,\mathbf{z}_1 \qquad \text{(C.12)}$$

with $\mathbf{H}$ as a matrix of damper impedances, $\mathbf{H} = \left(\mathbf{K}_{\mathbf{SFD}} - \omega^2 \mathbf{M}_{\mathbf{SFD}} + i\,\omega \mathbf{C}_{\mathbf{SFD}}\right)$. Eq. (C.12) provides two equations for determination of four impedance coefficients. Hence, in the numerical simulation, an orbital path with the same amplitudes is specified but with a *negative* frequency, ω<0 (clockwise whirl motion).

Next, the computational program calculates the SFD time varying reaction force for the new orbital path and delivers the fundamental Fourier components of motion and forces, i.e. $\mathbf{z_2}$ and $\mathbf{F_2}$. The specified orbital paths (forward and backward whirl orbits) ensure linear independence of the two reaction forces. Thus, using the two sets of results, write Eq. (C.12) as

$$\begin{bmatrix}\mathbf{F}_1 & \mathbf{F}_2\end{bmatrix} \approx \mathbf{H}\begin{bmatrix}\mathbf{z_1} & \mathbf{z_2}\end{bmatrix} \qquad \text{(C.13)}$$

at a particular frequency, say ω_k. Thus,

$$\mathbf{H}_{(\omega_k)} = \begin{bmatrix}\mathbf{F}_1 & \mathbf{F}_2\end{bmatrix}\begin{bmatrix}\mathbf{z_1} & \mathbf{z_2}\end{bmatrix}^{-1} \qquad \text{(C.14)}$$

delivers the impedance coefficients H_{XX}, H_{YY}, H_{XY}, H_{YX} at ω_k. The analysis stacks impedances for a set of frequencies ($\omega_{k=1,2,\ldots N}$) from which, by linear curve fits, one determines

$$\begin{aligned}\mathbf{K}_{\mathbf{SFD}} - \omega^2 \mathbf{M}_{\mathbf{SFD}} &\leftarrow \mathrm{Re}(\mathbf{H}) \\ \omega\,\mathbf{C}_{\mathbf{SFD}} &\leftarrow \mathrm{Im}(\mathbf{H})\end{aligned} \qquad \text{(C.15)}$$

Note that the numerical analysis follows an identical procedure as in the experimental identification of the test data. The computer program developed can be thought as a virtual tool to perform parameter identification in SFDs.

The goodness of the orbit-analysis derived SFD parameters is determined from the energy dissipated over one cycle of whirl motion. That is, over one period (T=2π/ω), the work performed by the SFD reaction force is

$$W_c = \oint \mathbf{dx}^{\mathbf{T}} \bullet \mathbf{F} = \oint_T \left(F_X\,\dot{x} + F_Y\,\dot{y}\right) dt \qquad \text{(C.12)}$$

[4] The validity of the assumption will be verified later with more examples as well as benchmarking against test data.

Using the linearized model, $\mathbf{F} = \mathbf{F}_{\mathbf{static}} + \mathbf{F}_{\mathbf{dyn}}$; $\mathbf{F}_{\mathbf{dyn}} \approx \mathbf{F}_1 e^{i(\omega t+\phi)}$,

$$W_c = \oint \dot{\mathbf{z}}^{\mathbf{T}} \bullet \left(\mathbf{F}_{\mathbf{static}} + \mathbf{F}_{\mathbf{dyn}} \right) dt = \oint \dot{\mathbf{z}}^{\mathbf{T}} \bullet \mathbf{F}_{\mathbf{static}} \; dt + \oint \dot{\mathbf{z}}^{\mathbf{T}} \bullet \mathbf{F}_{\mathbf{dyn}} \; dt = W_S + W_{dyn} \qquad \text{(C.13)}$$

The work performed by the static components of the bearing force is nil, i.e.

$$W_S = \oint \left(\dot{\mathbf{z}}^{\mathbf{T}} \bullet \mathbf{F}_{\mathbf{static}} \right) dt = \oint \left(F_{X_S} \dot{x} + F_{Y_S} \dot{y} \right) dt = F_{X_S} \oint \dot{x} \, dt + F_{Y_S} \oint \dot{y} \; dt = 0 \qquad \text{(C.14)}$$

since the whirl motion describes a full closed orbit with $x = x_c \, e^{i(\omega t+\phi)}$, $y = y_c \, e^{i(\omega t+\phi)}$.

Using the estimated linear force coefficients, the work is

$$W_{dyn\_linear} \sim \oint \left(\dot{\mathbf{z}}^{\mathbf{T}} \bullet \mathbf{F}_1 \right) dt = \oint \left(\dot{\mathbf{z}}^{\mathbf{T}} \bullet \left[\mathbf{K}_{\mathbf{SFD}} \, \mathbf{z} + \mathbf{C}_{\mathbf{SFD}} \, \dot{\mathbf{z}} + \mathbf{M}_{\mathbf{SFD}} \, \ddot{\mathbf{z}} \right] \right) dt \qquad \text{(C.15)}$$

The ratio $\left(W_{dyn\_linear} / W_c \right)$ will provide a measure of how well the estimated linear model reproduces the actual work (energy dissipated).

Further analysis and correlation to the experimental measurements will appear in the coming months.